ICARUS **120,** 119–139 (1996)
ARTICLE NO. 0041

Geology of 243 Ida

R. Sullivan, R. Greeley, and R. Pappalardo

Department of Geology, Box 871404, Arizona State University, Tempe, Arizona 85287-1404
E-mail: sullivan@asuws2.la.asu.edu

E. Asphaug, J. M. Moore, and D. Morrison

Space Sciences Division, NASA-Ames Research Center, Moffett Field, California 94035-1000

M. J. S. Belton

National Optical Astronomy Observatories, 950 N. Cherry Avenue, Tucson, Arizona 85719

M. Carr

Branch of Astrogeologic Studies, MS-946, United States Geological Survey, 345 Middlefield Road, Menlo Park, California 94025

C. R. Chapman

Planetary Science Institute, 620 N. 6th Street, Tucson, Arizona 85705

P. Geissler and R. Greenberg

Lunar and Planetary Laboratory, University of Arizona, Tucson, Arizona 85721

James Granahan

Hawaii Institute of Geophysics, University of Hawaii at Manoa, 2525 Correa Road, Honolulu, Hawaii 96822

J. W. Head III

Department of Geological Sciences, Box 1846, Brown University, Providence, Rhode Island 02912

R. Kirk and A. McEwen

United States Geological Survey, 2255 N. Gemini Drive, Flagstaff, Arizona 86001

and

P. Lee, P. C. Thomas, and J. Veverka

Center for Radiophysics and Space Research, Cornell University, Ithaca, New York 14853-6801

Received April 3, 1995; revised August 21, 1995

The surface of 243 Ida is dominated by the effects of impacts. No complex crater morphologies are observed. A complete range of crater degradation states is present, which also reveals optical maturation of the surface (darkening and reddening of materials with increasing exposure age). Regions of bright material associated with the freshest craters might be ballistically emplaced deposits or the result of seismic disturbance of loosely-bound surface materials. Diameter/depth ratios for fresh craters on Ida are ~1 : 6.5, similar to Gaspra results, but greater than the 1 : 5 ratios common on other rocky bodies. Contributing causes include rim degradation by whole-body "ringing," relatively thin ejecta blankets around crater rims, or an extended strength gradient in near-surface materials due to low gravitational self-packing. Grooves probably represent expressions in surface debris of reactivated fractures in the deeper interior. Isolated positive relief features as large as 150 m are probably ejecta blocks related to large impacts. Evidence for the presence of debris on the surface includes resolved ejecta blocks, mass-wasting scars, contrasts in color and albedo

of fresh crater materials, and albedo streaks oriented down local slopes. Color data indicate relatively uniform calcium abundance in pyroxenes and constant pyroxene/olivine ratio. A large, relatively blue unit across the northern polar area is probably related to regolith processes involving ejecta from Azzurra rather than representing internal compositional heterogeneity. A small number of bluer, brighter craters are randomly distributed across the surface, unlike on Gaspra where these features are concentrated along ridges. This implies that debris on Ida is less mobile and/or consistently thicker than on Gaspra. Estimates of the average depth of mobile materials derived from chute depths (20–60 m), grooves (≥30 m), and shallowing of the largest degraded craters (20–50 m minimum, ∼100 m maximum) suggest a thickness of potentially mobile materials of ∼50 m, and a typical thickness for the debris layer of 50–100 m.

1. INTRODUCTION

The Galileo spacecraft flew past the asteroid 243 Ida on August 28, 1993, while en route to Jupiter (O'Neil *et al.* 1992). During the Ida encounter the solid-state imaging (SSI) system obtained images from ranges of 240,350 km to 2390 km over 5.5 hr. During this time Ida's brief rotation period of 4.63 hr (Binzel *et al.* 1993a) afforded good longitudinal coverage, although at widely varying resolutions. Twenty-one SSI observation sequences were executed successfully during the encounter, including combinations of six visible and near-infrared filters. All images were recorded on the spacecraft for transmission to Earth later using the low-gain antenna, beginning with five high resolution (31–38 m/pixel) clear-filter images (Belton *et al.* 1994). A single limb-grazing 25 m/pixel clear-filter image was returned later, along with color and other data (Belton *et al.* 1996). This paper describes and analyzes the surface features of Ida visible in these images, and discusses implications for the geological evolution of the asteroid.

Ground-based observations prior to the Galileo flyby established that Ida is an S-class asteroid and a member of the Koronis dynamical family (Chapman *et al.* 1975, Chapman *et al.* 1989, Gaffey *et al.* 1993). The S-class is the second most populous asteroid class in the main asteroid belt and shows considerable spectral diversity. Gaffey *et al.* (1993) divided 39 S-class asteroids into seven subclasses; in their taxonomy Ida belongs to class S(IV), the most abundant subtype in their sample. Class S(IV) asteroids are distinguished by spectral absorption features diagnostic of olivine and orthopyroxene. Koronis family members are all S-types in a zone dominated by C-types (Gradie *et al.* 1979, Gradie *et al.* 1989), consistent with the hypothesis that the family originated from the disruption of a larger parent body (Kuiper 1950, Weisel 1978). Binzel (1988) modeled the collisional evolution of the Koronis family from lightcurve amplitudes and the distribution of rotation periods, and concluded that the Koronis family was dynamically immature compared with the Eos family. Although an absolute age since disruption of the Koronis parent body could not be specified, the possibility that Ida is young compared with the age of the solar system was an interesting possibility to be tested by Galileo data.

Ground-based studies have revealed only limited spectral diversity among Koronis family members (Gradie *et al.* 1979, Zellner *et al.* 1985, Binzel *et al.* 1993b). If major compositional heterogeneities exist within and between Koronis family asteroids, they might be too compositionally subtle or volumetrically insignificant to be resolved with ground-based data. An important goal of the Ida flyby was to search for smaller scale compositional diversity on Ida.

SSI images were analyzed by Thomas *et al.* (1996) to develop a model for the shape of Ida. The asteroid shape deviates significantly from a best fit ellipsoid (29.9 × 12.7 × 9.3 km) and cannot be characterized as facets with intervening rounded ridges, as was the case for Gaspra (Thomas *et al.* 1994, Carr *et al.* 1994). Ida is roughly crescent shaped, with more volume concentrated asymmetrically at one end rather than in the center. The basic crescent shape of Ida is modified by several ∼10 km diameter impact craters, saddles which might be impact craters that are large relative to local target curvature, several asymmetric depressions which might be related to oblique impacts or spallation, and ridges (Thomas *et al.* 1996). Imposed upon this topography are smaller features, including impact craters, albedo markings, and grooves, which together are the basis for most of the geological analysis of this paper. Proposed IAU feature names are shown in Fig. 1, and the nomenclature system is discussed by Belton *et al.* (1996). High-resolution views of Ida (Figs. 2–5) afford the opportunity to (1) investigate the nature of impact cratering in a very low gravity environment, (2) evaluate variations of color and brightness across the surface and their relation to specific morphological features, (3) assess the presence, character, and mobility of surface debris, (4) relate ground-based observations to aspects of the surface seen by spacecraft, and (5) compare surface features of Ida with other small bodies imaged by spacecraft.

2. COLOR VARIATIONS ACROSS THE SURFACE

2.1. Data Sets

The Galileo SSI returned nine sets of color observations acquired at phase angles from 19.5° to 26.5° during the approach to Ida. Most of these color sets consist of images taken through the 0.41, 0.56, 0.89, and 0.99 μm filters. One color set includes a 0.67 μm filter, and another (the highest-resolution color set) includes the 0.76 μm filter. These nine sets of observations provide

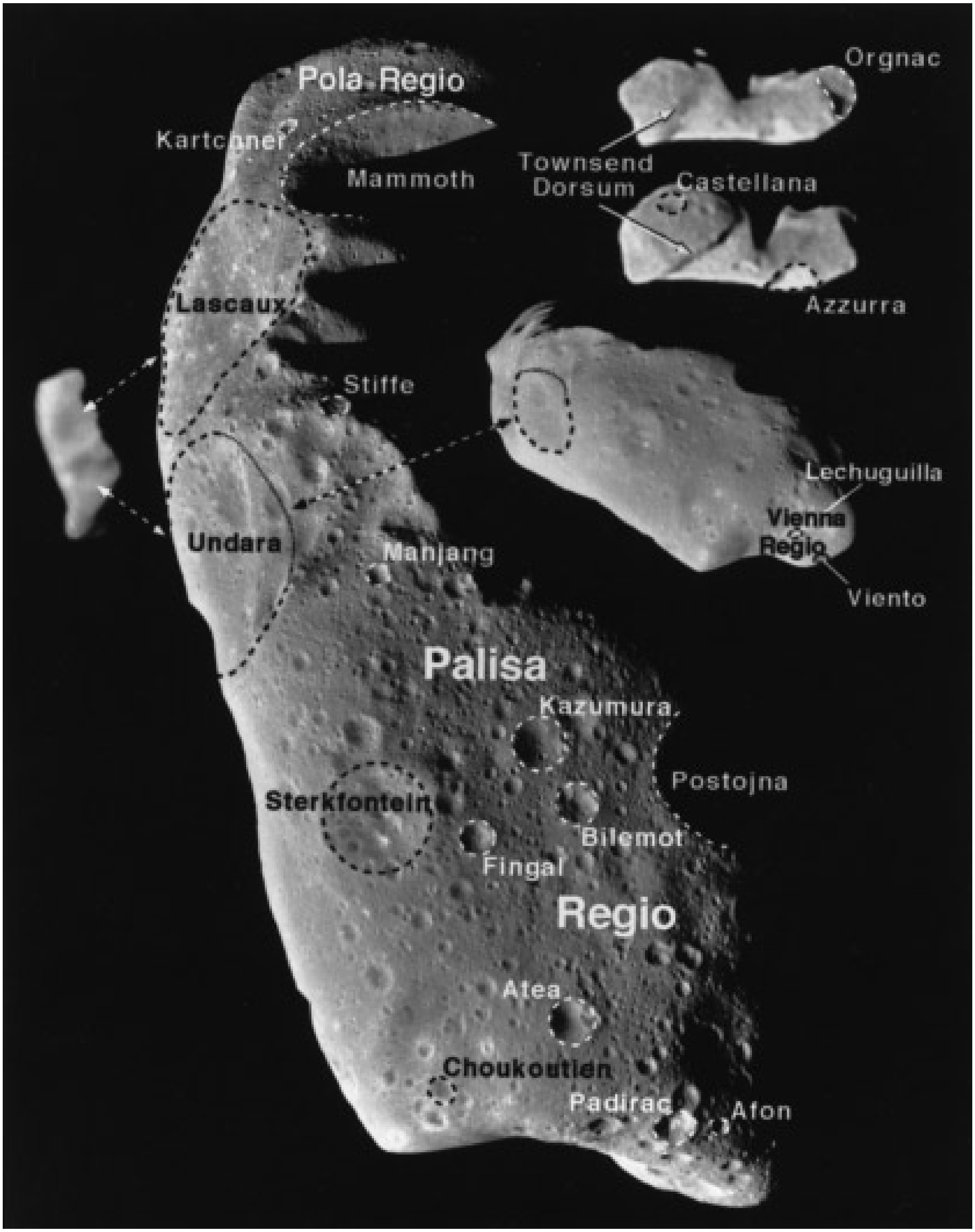

FIG. 1. Proposed IAU names for features on Ida. See Belton *et al.* (1996) for details of the nomenclature. Figs. 2–5 and 9 share the same orientation.

complete coverage of illuminated regions of Ida through about one full rotation. See Veverka *et al.* (1996) and Belton *et al.* (1996) for more detailed information on these images. A color-ratio composite showing nine views of Ida is shown in Fig. 6.

The most useful color filters for mapping spectral units on S-type asteroids in the spectral range 0.4–1.0 μm are (1) a pair of filters mapping ultraviolet absorption (such as 0.41 and 0.56 μm), (2) a pair of filters covering the visible spectral region (such as 0.56 and 0.67 or 0.76 μm), (3) a pair of filters that map the 1-μm band depth (such as 0.76 and 0.99 μm), and (4) filters that can be used to constrain the wavelength minimum of the 1-μm band (such as 0.89 and 0.99 μm). Only four filter images (0.41, 0.56,

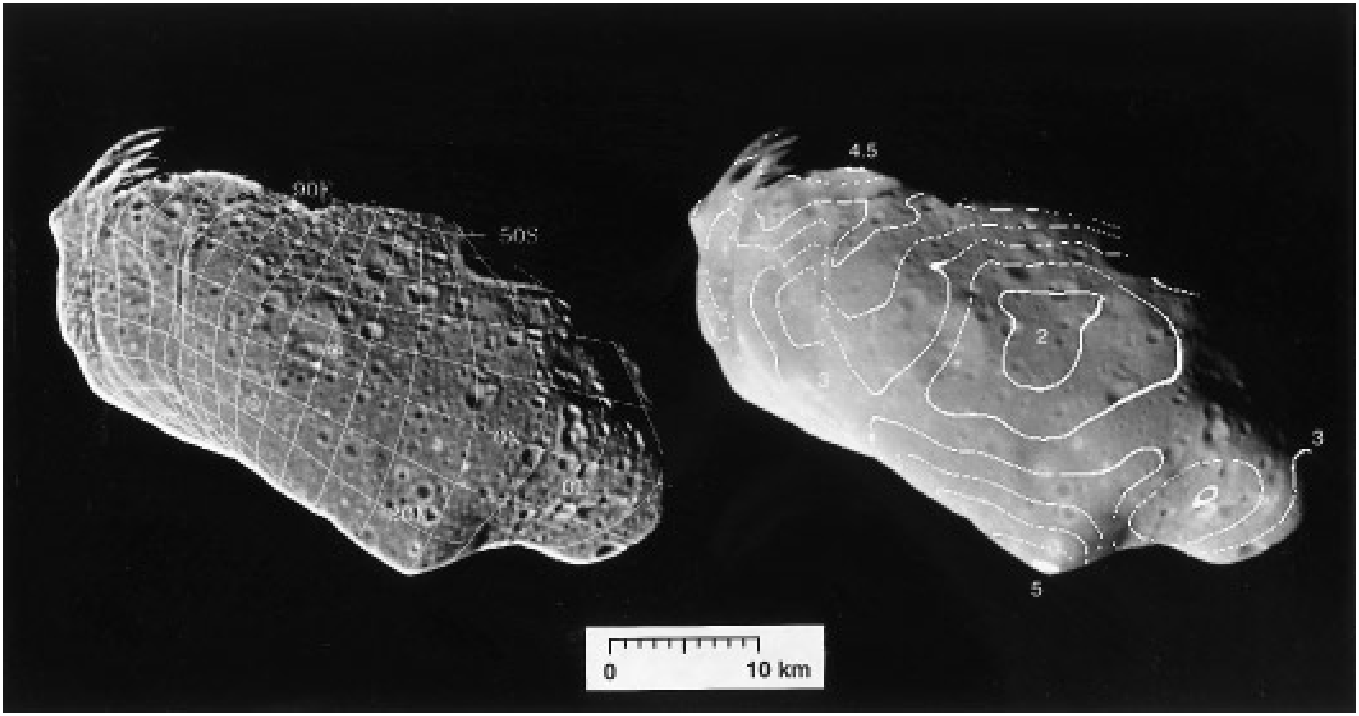

FIG. 2. Coordinates and dynamic height contours for s0202561278. Dynamic height contours in km (calculated in Thomas *et al.* 1996) are everywhere normal to downslope acceleration directions including the effect of accelerations due to the rotation of the asteroid. Phase angle is 26.4°, and resolution is 111 m/pixel.

0.89, 0.99 μm) are available for all rotational views. Determination of the 1-μm band depth is best accomplished with the 0.76-μm filter, which measures the continuum, but this filter is available in only the highest resolution color view. However, from the high-resolution color set we can see that the 0.76/0.99 μm ratio correlates with visible color ratios such as 0.41/0.56 μm, and the 0.56/0.99 μm ratio appears to map the same spectral units as the 0.76/0.99 μm ratio.

2.2. *Description of Color Variations*

The wavelength position of the 1-μm absorption is important because it is controlled entirely by mineralogy, independent of soil maturity or grain size effects (Adams 1974, Gaffey 1976). For Ida, the 0.89 and 0.99 μm images are all highly correlated. The histogram of Ida's 0.89/0.99 μm ratio image is narrow, with a standard deviation of only about 2%, and much or all of this variation appears to be due to noise. This indicates that any mineralogical heterogeneity that could affect the wavelength position of the 1-μm pyroxene–olivine absorption on the imaged portions of Ida is minor, implying no strong variations from region to region in the calcium abundance of pyroxenes or in the pyroxene/olivine ratio (Adams 1974, Cloutis *et al.* 1986, Cloutis and Gaffey 1991). This is also the case for Gaspra and for Ida's satellite, Dactyl. However, this does not exclude the possibility that Ida could be a composite of compositionally-related Koronis-family fragments (Binzel *et al.* 1993b). The 0.89/0.99 μm ratio is 8% higher for Gaspra than for Ida or Dactyl, consistent with Gaspra's olivine-rich composition.

Color variations on Ida are apparent in its visible color (0.41/0.56 μm, 0.41/0.67 μm, or 0.41/0.76 μm ratio) and 1-μm band depth (0.76/0.99 μm or 0.76/0.89 μm ratio, also approximated by 0.56/0.99 μm ratio). The relatively blue areas (higher 0.41/0.56 μm, 0.41/0.67 μm, or 0.41/0.76 μm) are correlated with regions with a deeper 1-μm band (higher 0.76/0.99 μm or 0.56/0.99 μm) and with areas that have higher albedos. These are the same spectral relations seen on Gaspra (Belton *et al.* 1992, Helfenstein *et al.* 1994) and, in much more pronounced form, on the Moon (Adams and McCord 1971). We will refer to the areas that have relatively high 0.41/0.56 μm and 0.76/0.99 μm (or 0.56/0.99 μm) ratios on both Gaspra and Ida as "blue" units (these areas appear blue in the color-ratio composite, Fig. 6).

In addition to the different 0.89/0.99 μm ratio between Gaspra and Ida, Gaspra is also significantly bluer (39% higher 0.41/0.56 μm ratio) and has a 10% deeper 1 μm band (0.76/0.99 μm ratio) (see Belton *et al.* 1996). This is consistent with S-class asteroids with diameters less than

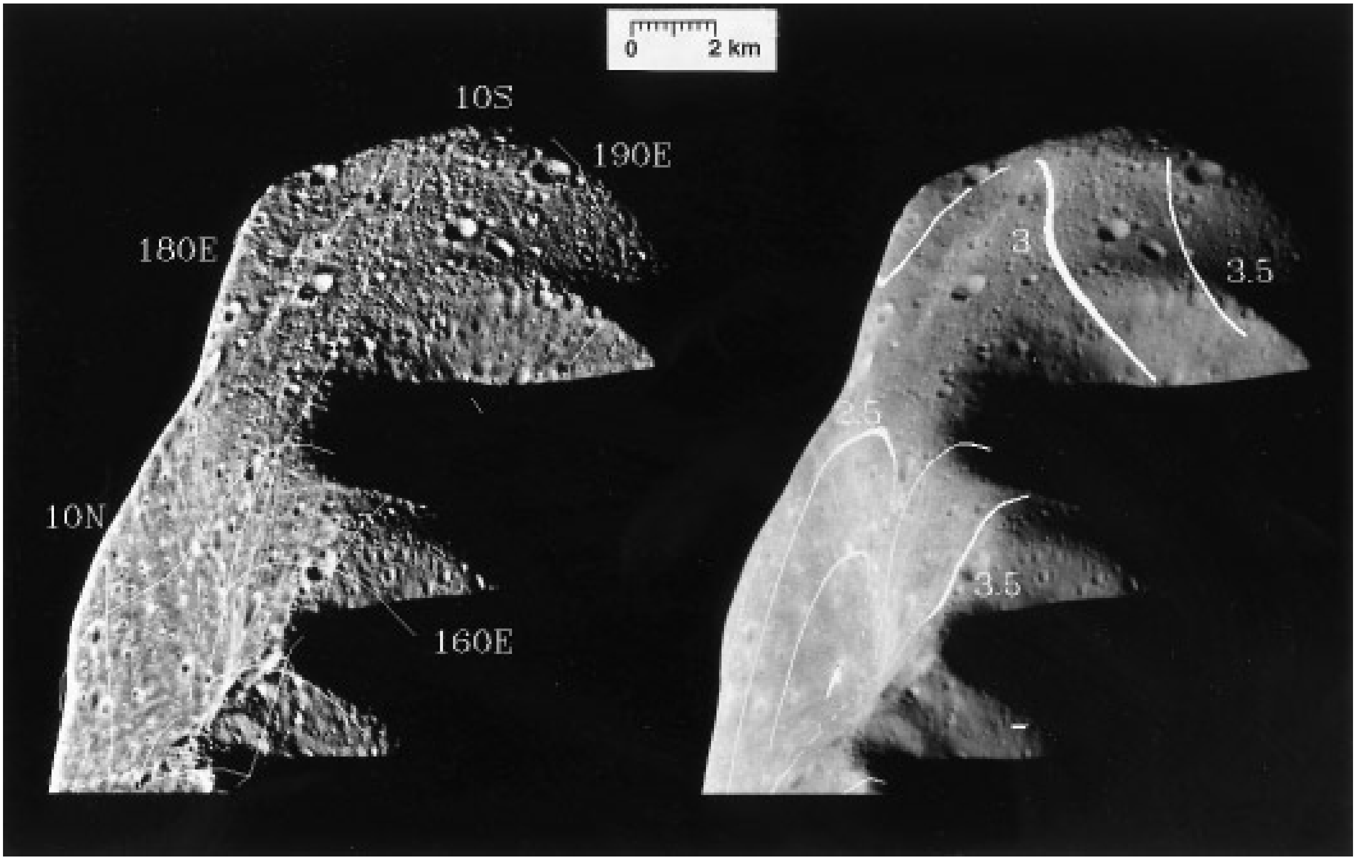

FIG. 3. Coordinates and dynamic height contours for s0202562439. Dynamic height contours in km (calculated in Thomas *et al.* 1996) are everywhere normal to downslope acceleration directions including the effect of accelerations due to the rotation of the asteroid. Phase angle is 59.1°, and resolution is 31 m/pixel.

100 km having 1 μm band depths related inversely to their diameters (Gaffey *et al.* 1993).

2.3. Color Unit Distribution

There is a clear difference between Gaspra and Ida in the regional occurrence of color units. The blue unit (and blue craters) on Gaspra are concentrated on topographic ridges (Belton *et al.* 1992, Carr *et al.* 1994, Helfenstein *et al.* 1994), but this is not the case on Ida (see also Veverka *et al.* 1996). In addition to randomly distributed blue craters, there is a large blue region (or regions) in Ida's northern hemisphere. Because of Ida's shape and the geometry at which Galileo imaged Ida, there appear to be two blue regions in Ida's northern hemisphere; we cannot see if they are connected. The blue regions occur in the ''neck'' between Ida's two major regions, but our view of the neck region is blocked when viewing from a direction approximately parallel to Ida's long axis. Both apparent blue regions are partly bounded by the large ridge on Ida (cf. Fig. 3a of Thomas *et al.* 1996) on its southern margin. The northern margin (if it exists) cannot be seen. This large blue region occurs in areas of average dynamic height, slope, and gravitational acceleration (Figs. 3c–3e of Thomas *et al.* 1996). This northern blue unit is spectrally indistinguishable from bright, fresh crater materials, which suggests that it is related to regolith processes rather than large-scale compositional heterogeneity. However, the unit clearly does not correspond to protruding topographic ridges where downslope regolith movements driven by small impacts could be expected, as is the case on Gaspra. The only morphologic clues to the origin of this spectral unit are its association with a ridge spanning nearly 150° of longitude that might mark a planar structure through Ida (Thomas *et al.* 1996) and its proximity to the large crater Azzurra, which appears to be less degraded than other craters of similar size. Geissler *et al.* (1996) evaluated the hypothesis that the northern blue unit owes its origin to distribution of low velocity ejecta from Azzurra, and found an excellent correspondence between the calculated distribution of ballistically emplaced particles from Azzurra and the blue region.

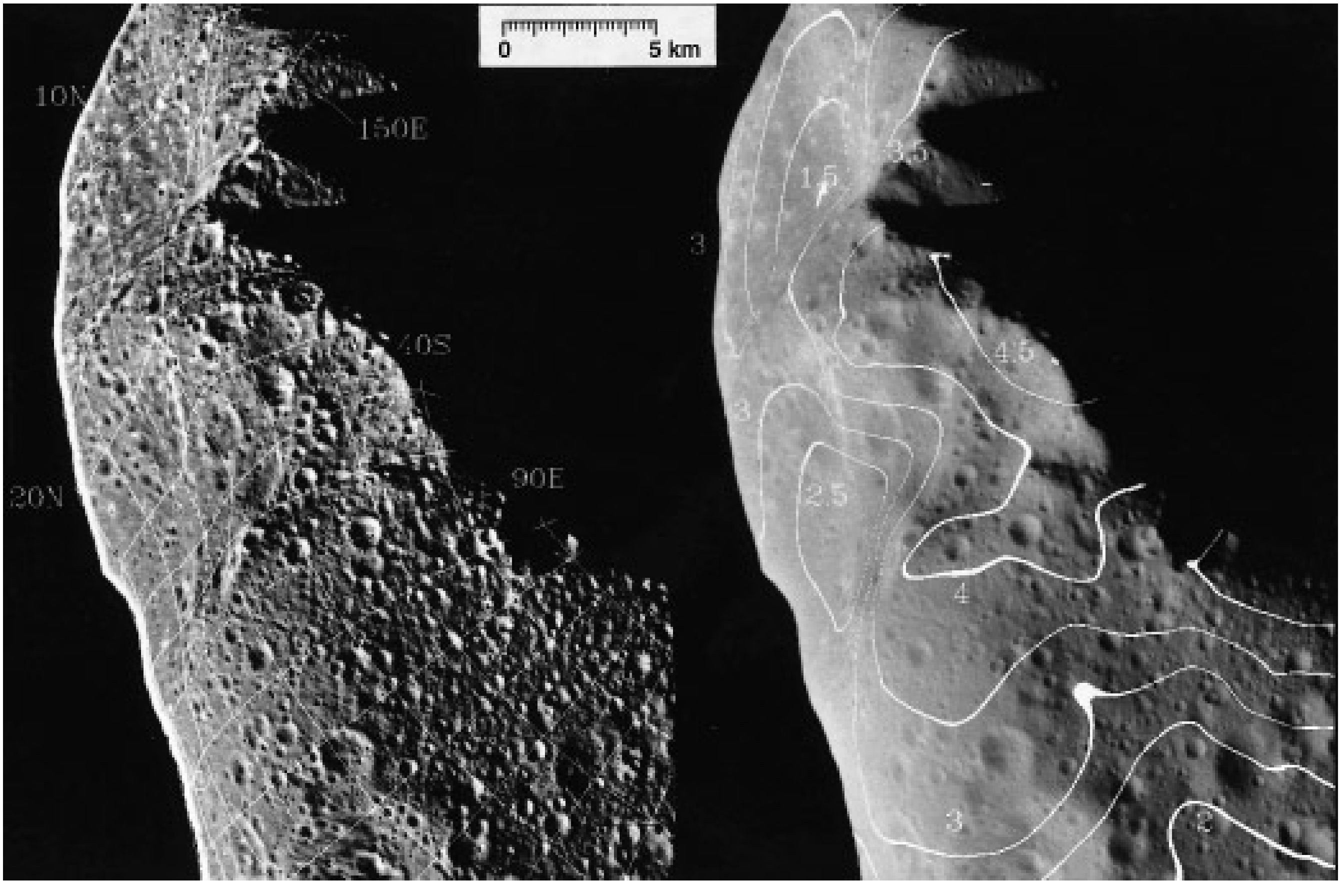

FIG. 4. Coordinates and dynamic height contours for s0202562339. Dynamic height contours in km (calculated in Thomas *et al.* 1996) are everywhere normal to downslope acceleration directions including the effect of accelerations due to the rotation of the asteroid. Phase angle is 50.6°, and resolution is 37 m/pixel.

3. IMPACT CRATERS

3.1. Crater Morphology

The morphology and topography of the surface of Ida is dominated by impact craters ranging in size from 12 km to the limit of resolution (25 m/pixel). The craters have "simple" morphology—i.e., they are bowl-shaped, with no discernible break in slope between walls and floors. Generally, features such as flat floors, slump-terraced walls, central peaks or pits, central peak rings, or multiple rings are absent. On the Moon, the transition between simple and complex crater morphologies occurs at diameters of about 16 km in the maria and 21 km in the highlands (Pike 1980). On other bodies, the simple-to-complex transition occurs at smaller diameters with increasing surface gravity, so complex crater morphologies are not expected for craters in the size range observed on Ida. One exceptional feature is the asymmetric, relatively fresh (undegraded) 1400 m diameter crater Fingal (13°S, 41°E, Figs. 1 and 5), which has a straight wall segment and, on one side only, a sharp break in slope between the crater floor and the interior wall. The floor of this crater has a rough texture, suggestive of several superposed impact craters, but details are difficult to resolve. Fingal is probably the result of an oblique impact, and is not representative of a simple-to-complex morphology transition because larger (albeit more degraded) craters do not have flat floors.

There is a complete continuum of crater degradation states at all observable sizes (see also Chapman *et al.* 1996). Most craters have irregular rims and/or superposed impacts and are obviously degraded. The freshest craters have sharp, circular rims that do not show damage from subsequent impacts. However, distinguishing the most pristine craterforms—especially at smaller sizes—is limited by image resolution. Many smaller craters that appear pristine in the images probably have significant rim and cavity degradation that cannot be detected.

A small minority of craters that appear pristine have

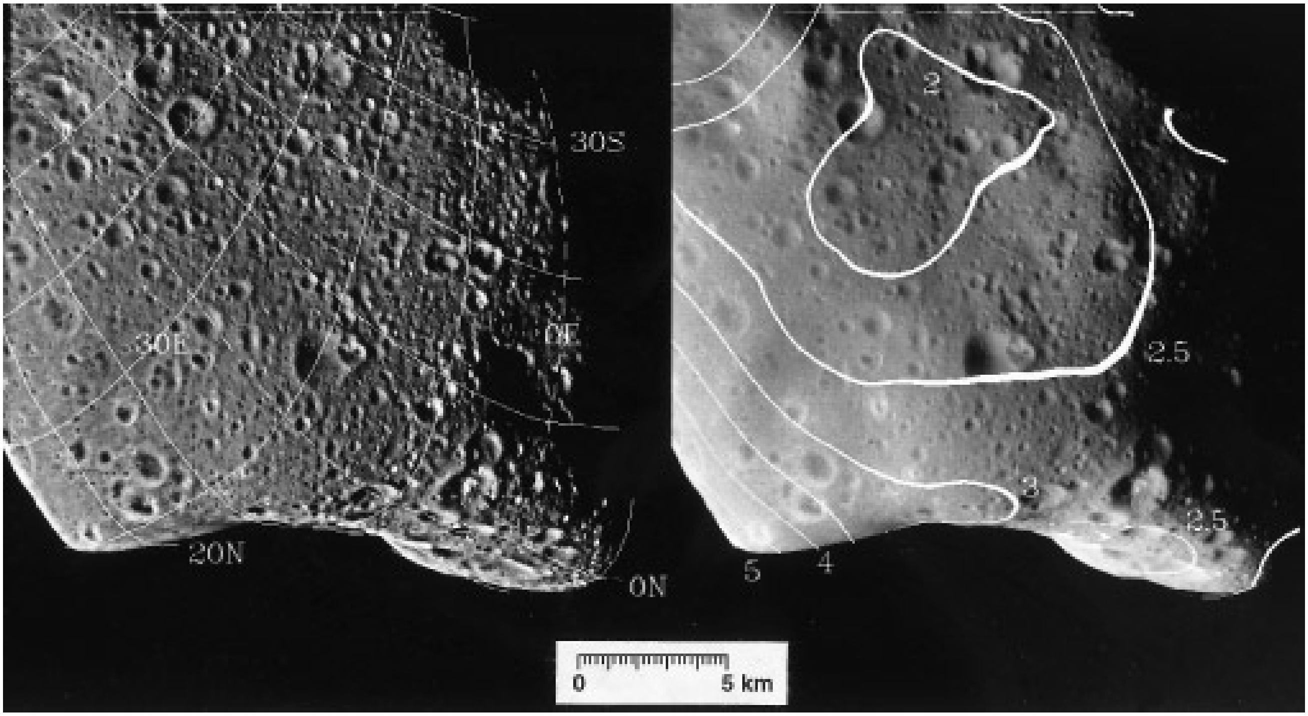

FIG. 5. Latitude and longitude coordinates and dynamic height contours in km for image s0202562313, as calculated in Thomas *et al.* (1996). Dynamic height contours are everywhere normal to downslope acceleration directions including the effect of accelerations due to the rotation of the asteroid. Phase angle is 48.7°, and resolution is 38 m/pixel.

high-albedo material distributed over interiors and in irregular zones around rims. These bright zones have diffuse boundaries that vary in extent but commonly lie within one crater radius of crater rims. High-albedo crater deposits rarely occur as crater rays; only one crater with one or perhaps two short rays has been identified. Smaller examples of craters with associated bright deposits are more numerous than larger examples. The fraction of pristine-appearing craters that have high-albedo deposits is difficult to establish because (1) they are rare, (2) identification of smaller examples is biased by uneven resolution coverage, and (3) variation of incidence and emission angles across the high-resolution mosaic affects the visibility of high albedo materials. For the same reasons, it is not possible to compile meaningful statistics about the variations of size and brightness of high-albedo zones around craters. All that can be said is that the size (normalized to crater diameter) and average brightness of high-albedo zones vary among craters of similar diameter, and seem positively correlated.

High-albedo crater materials also are distinguished by their color. Comparison of clear-filter images with color data shows that the location and extent of high-albedo crater materials correlates well with localized bluer-than-average zones. Figure 7 compares SSI spectra, calibrated according to Helfenstein *et al.* (1996), of two nearby areas of Ida. Bright materials associated with a small crater (2°S, 52°E, Figs. 2 and 5) in Sterkfontein (Fig. 1) are bluer than a patch of average cratered terrain nearby; the 0.41/0.56 μm ratio is higher and the 1-μm absorption is deeper for the bright crater deposits than for the surrounding terrain. Similar color relationships were found for some undegraded craters on Gaspra, although the freshest craters on Gaspra are not distinguished by higher albedo (Belton *et al.* 1992, Helfenstein *et al.* 1994, Carr *et al.* 1994).

The most likely origin for the bright, bluer-than-average crater deposits on Ida is that these materials represent fresh deposits from some of the youngest impacts on the surface. The observation that high-albedo craters always have undegraded rims (but not vice versa) implies that craters on Ida form initially as brighter- and bluer-than-average features that decrease in brightness and redden to typical background values in the first stage of their morphological lifetimes. This transition is completed before crater rims are altered perceptibly by subsequent impacts. A similar sequence characterizes crater degradation and erosion on the Moon, where high albedo deposits such as rays fade to invisibility as the first step of crater degradation (Shoemaker and Hackman 1962, Pieters *et al.* 1985). The rates at which high-albedo materials lose their distinctiveness probably differ between the Moon and Ida, due in part to differences in micrometeorite fluxes and solar wind fluxes between the two surfaces. For several reasons (see discussion in Section 6), surface materials on Ida might never evolve to the same degree of optical maturity as on the Moon (cf. Matson *et al.* 1977), so bright materials on Ida might undergo less alteration than on the Moon before losing their distinctiveness.

It is unlikely that bright craters derive their distinguishing albedos and colors from excavation into compositionally distinct target materials. The fact that smaller bright craters are more abundant than larger ones is consistent with bright crater materials reflecting merely youth and nothing more. If bright, bluer craters marked the location of anomalous subsurface deposits, these craters should exist in all degradation states. Instead, bright, bluer craters with only sharp rims are seen. These distinctive craters are not grouped in clusters (that would be consistent with a large, compositionally distinct component buried beneath a thin blanket of debris); even the smallest examples seen at high resolution are scattered randomly about the surface, intermingled with craters having no distinctive albedo or color. We conclude that cratering on Ida produces deposits of brighter- and bluer-than-average materials that darken and redden to background levels as the first stage of crater degradation. As craters continue to age, their rims become more irregular from the superposition of subsequent impacts, and their depths decrease until they are hardly recognizable, even at low illumination angles.

We consider two possible mechanisms for generating the bluer, brighter units associated with the freshest impact craters. First, these units might simply represent optically immature ejecta blankets excavated during impact and deposited immediately around the crater rim, burying more optically mature (darker and redder) target material. The volume of ejecta deposited adjacent to a crater rim on Ida might be small, especially if target strength is influential in the excavation process and ejecta velocities are high. However, Ida's low gravity might cause an optically maturing surface layer of relatively loosely held debris to be especially fragile, and subject to widespread disturbance and resetting by even small amounts of ballistically emplaced materials concentrated around the rim. A second possibility is that seismic disturbances associated with the impact event might be sufficient to disrupt a maturing optical layer in the vicinity of the crater rim. Seismic surface accelerations greater than 1 cm sec^{-2} would be sufficient not only to churn and disrupt loose material in the optical surface layer, but to loft loose materials into short ballistic trajectories (Arnold, in discussion following Chapman 1978, Cintala *et al.* 1978, 1979).

These hypotheses were investigated in a series of numerical simulations comparing ranges of ballistic ejecta with areas of seismic disturbance around craters on Ida (Asphaug *et al.* 1996). Projectiles ranging from 2 to 60 m in diameter were impacted at 3.55 km/sec, producing simulated craters ranging from 60 m to 8 km in diameter. The smaller crater simulations are more comparable to bright craters observed in SSI images. Results of the simulations confirmed the expectation that ballistically emplaced deposits from the smallest craters on Ida should be diffuse, widespread, and thus difficult to recognize, as a consequence of target strength influencing the excavation process at smaller diameters (e.g., Cintala *et al.* 1978, 1979, Housen *et al.* 1979a, 1979b, Housen *et al.* 1983, Veverka *et al.* 1986, O'Keefe and Ahrens 1993). Seismic accelerations from the same simulated impacts are predicted to disturb surface materials several crater radii outward (Asphaug *et al.* 1996). Results of these calculations and comparison with observations of the surface did not eliminate either mechanism as a possible explanation for bright, blue materials around the freshest craters on Ida. Evidence from the images is statistically insufficient to conclude that one mechanism predominates (see Figs. 4 and 5 in Asphaug *et al.* 1996). Both ballistic ejecta emplacement and seismic disturbance could contribute to the appearance of materials around the freshest craters.

Although a continuum of crater degradation states is found on Ida, it is not clear whether all degradation states are present at all locations (see also Chapman *et al.* 1996). Small sample areas and nonuniform resolution and lighting/viewing geometry make recognition of local variations in crater density or crater morphology tentative, but a few areas seem anomalous. Pola Regio (10°S, 185°E) is favorably illuminated for recognition of subtle topographic variations, but is nearly devoid of heavily degraded craters

FIG. 6. Color ratio composite showing one rotation of Ida, with all views shown to the same scale. North is down. Rotation of the asteroid is indicated in nine views starting from the upper left, proceeding horizontally, and concluding in the lower right. The lower right view is the same as seen in Figs. 2 and 7. Each color view consists of SSI 0.41, 0.56, and 0.99 μm filter images merged with a high-pass filtered image to enhance topographic shading.

FIG. 7. Comparison of SSI five-color spectra of fresh, high-albedo crater material and average surface materials. The color composite shows the location of each spectral patch and is the same view as Fig. 2. Colors are 0.76/0.41 μm as red, 0.76/0.99 μm as green, and 0.41/0.76 μm as blue. A high-pass filtered version of the 0.76 μm image has been added to all three colors to show surface topography. Spectra are from data calibrated according to Helfenstein *et al.* (1996) and normalized to 0.56 μm. The "blue 1" spectrum is from a small bright crater with one or perhaps two short rays located within crater Sterkfontein; "red 1" is located in average terrain nearby. Error bars are standard deviations within each sample.

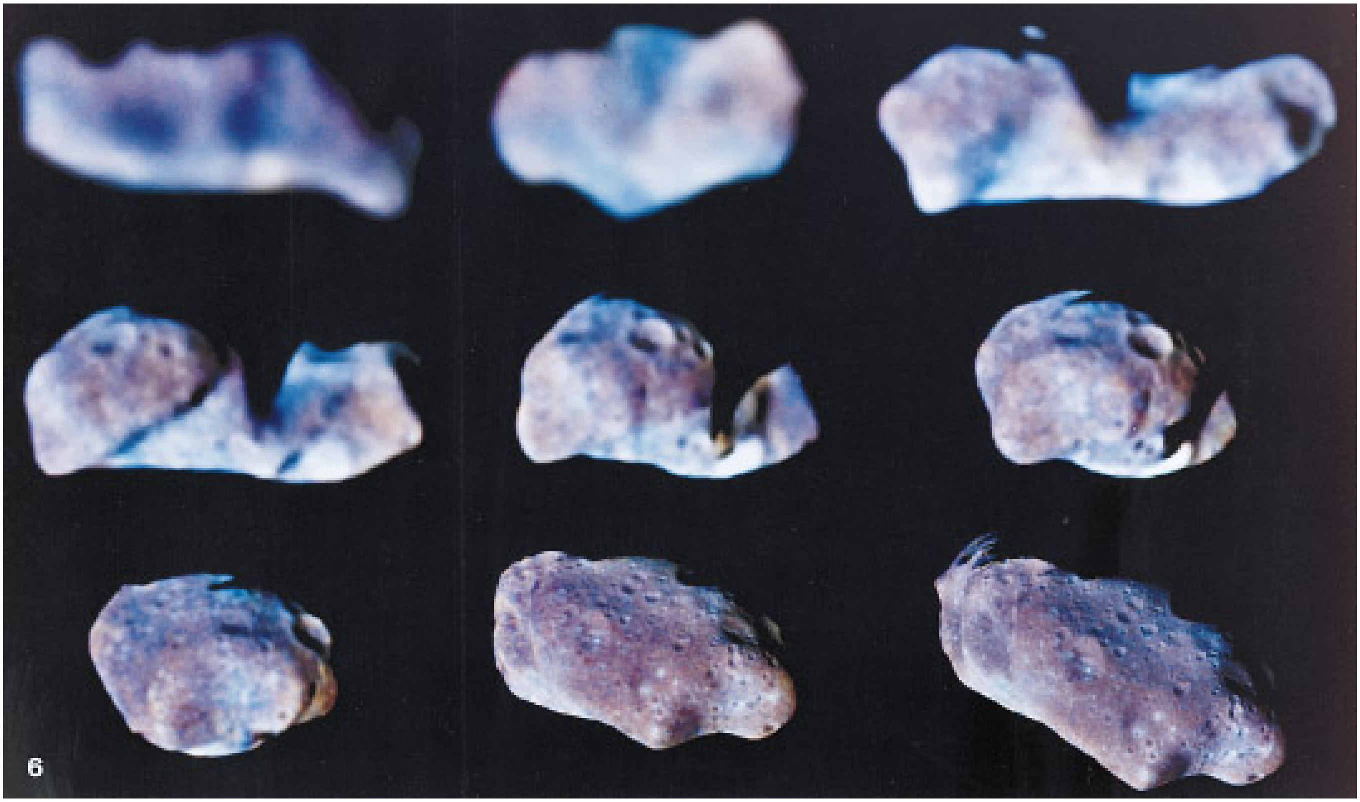
6

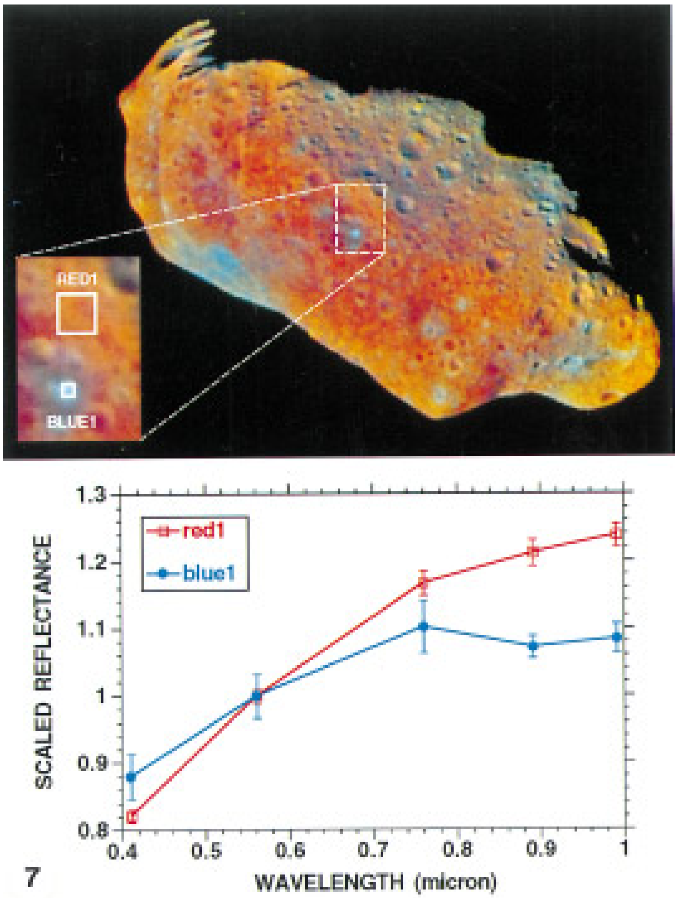
RED1
BLUE1
red1
blue1
SCALED REFLECTANCE
WAVELENGTH (micron)
1.3
1.2
1.1
1
0.9
0.8
0.4
0.5
0.6
0.7
0.8
0.9
1
7

compared with other regions of Ida. A second example of an anomalous area involves a protrusion at the 30°N, 20°E end of Ida (north of crater Choukoutien) that appears less cratered than other areas of the surface (compare with the protrusion at 350°E). At around 10°N, 18°E this relatively smooth protrusion makes a break in slope with a rougher surface to the south and west. Such a break in slope can form by deposition of materials in approximate accordance with the local geoid against the side of a more steeply projecting slope. Slopes drop steeply away from the 20°E protrusion (Figs. 2 and 5), so debris at the surface would be susceptible to migration away from this feature and into adjacent areas. This process might have left a lag of stronger-than-average materials in the area, resulting in smaller, less prominent craters compared with adjacent regions and giving the area its smoother, less-cratered appearance.

The low-gravity environments of small bodies such as Ida are natural laboratories for evaluating the influence of gravity and target strength on crater excavation and ejecta dispersal (Housen *et al.* 1983, Greenberg *et al.* 1994, Greenberg *et al.* 1996, Asphaug *et al.* 1996). Distinct ejecta blankets similar to continuous deposits surrounding lunar crater rims are not seen around craters on Ida (nor on Phobos, Deimos, or Gaspra). However, it is difficult to distinguish the limits of continuous ejecta blankets of similar-sized impact craters on the Moon under the same illumination and resolution conditions. Many fresh craters (and some of the largest degraded craters) on Ida do have raised rims making a distinct break in slope with surrounding terrain, but it is not clear how much of the raised rim height is due either to upwarped target material "bulked" by impact, or to the presence of a substantial ejecta blanket deposited onto the surface concentric to the rim.

3.2. Crater Depth/Diameter Ratios

The relationship between depths and diameters for craters on Ida is shown in Fig. 8. Measurements were made from profiles through photoclinometric topographic models of five areas on four clear-filter images with resolutions from 31 to 38 m/pixel. The photoclinometry data set for this analysis was prepared in a manner similar to that used by Carr *et al.* (1994), based on the method of Kirk (1987). The shape model from Thomas *et al.* (1996) was used as a basis for two-dimensional photoclinometric iterations employing a combined Lommell–Seeliger (lunar) and Lambertian photometric function in order to derive topography. The values of the lunar/Lambert weight L in this photometric function were chosen by least-squares fitting of pseudo-images shaded from the Thomas *et al.* model to the real images.

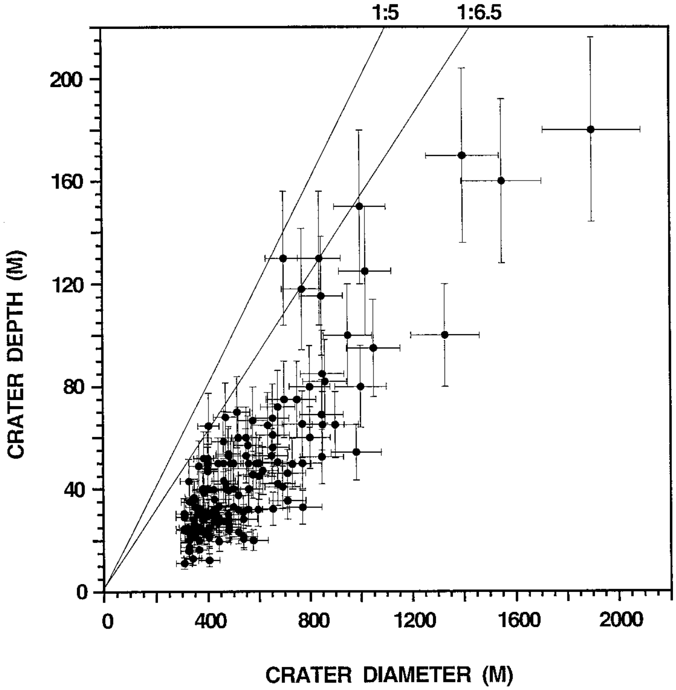

FIG. 8. Crater depth/diameter plot for 160 craters on Ida. Systematic errors in depth inherent in the photoclinometry algorithm are ≤10%, but other errors due to noise, miscalibration, and other sources are difficult to quantify. Estimate-of-error bars are 20% for crater depths and 10% for crater diameters. The slope defining the freshest crater depth/diameter ratio is not 1 : 5, but closer to 1 : 6.5

It was desirable to measure craters from a wide range of crater degradation states in addition to the freshest craters, but heavily degraded craters are more difficult to recognize in the images and to distinguish satisfactorily in topographic profiles. As a result, heavily degraded craters are underrepresented in the depth/diameter plot. Craters with the highest depth/diameter ratios generally have the freshest morphologies; these craters are bounded by a minimum depth/diameter ratio of about 1 : 6.5. Craters with increasingly degraded rims generally have lower depth/diameter ratios. The fresh crater 1 : 6.5 depth/diameter ratio obtained for Ida is similar to 1 : 7 obtained for Gaspra (Carr *et al.* 1994), but differs from the 1 : 5 ratios measured for fresh, simple craters on the Moon, Mercury, Mars, and Phobos (Gault *et al.* 1975, Malin and Dzurisin 1977, Cintala and Mouginis-Mark 1979, Thomas 1978, Pike 1980).

The 1 : 7 crater depth/diameter ratios for Gaspra and the 1 : 6.5 results for Ida were obtained using the same method, while the 1 : 5 depth/diameter ratios for Phobos were obtained from shadow measurements. Although a systematic error in our crater depth results is possible, we have considered several possible sources and regard such errors as unlikely. First, error could arise from intrinsic limitations of the photoclinometric algorithm. Second, "smoothing" in the images of craters (i.e., reduction of the apparent contrast between up- and down-sun slopes because of resolution limitations) would reduce apparent depths of the smallest craters. In order to evaluate these two possible sources of error, we performed a series of numerical simulations with the clinometry algorithm. A digital terrain model of an idealized lunar-like craterform with a 1:5 depth/diameter ratio was generated, and a shaded image of the craterform topography was created by applying parameters typical of the high-resolution images of Ida (a Lommell–Seeliger/Lambert photometric function with lunar weight parameter $L = 0.3$, a phase angle of 50°, and illumination from 25° off the sample axis). This image was subsampled by 2×2 averaging into images with crater diameter ranging from 2 to 128 pixels/diameter, and then two-dimensional photoclinometry was performed on these images. For crater diameters of 8 to 128 pixels, recovered depths showed errors ranging from +6% to −1% (i.e., depth/diameter ratios ranging from 1:5.29 to 1:4.95) with the larger craters being systematically shallower, suggesting a weak effect of iteration short of convergence in these tests. Premature termination of three-dimensional clinometric iterations before complete convergence probably was not a source of error in the Ida data, however, because the residuals on the clinometric fit typically showed good convergence for the overall shape of Ida, and convergence for local features such as small craters occurs much faster. In the clinometry tests, apparent depths of craters ≤4 pixels in diameter were clearly reduced by the low-resolution smoothing effect, so in our Ida data we measured only craters larger than 8 pixels. We therefore consider a systematic error of ≤10% in crater depths to be likely. The effects of nonsystematic errors independent of the photoclinometry algorithm (e.g., local albedo variations, miscalibration, and noise) are difficult to quantify, but these effects should not systematically bias results toward shallower or deeper crater depth measurements. Another possible source of error, not addressed by our numerical tests, would be an erroneous photometric function, which could lead to an incorrect relation between image contrast in craters and their inferred depth. However, the photometric function was obtained by fitting the overall shape model of Thomas *et al.* (1996) to the images, and this fit agreed with an independent lunar-Lambert fit (McEwen 1991) to a Hapke solution over a range of phase angles. The local photometry of craters on Ida might be different, but this seems rather improbable. We regard the 1:6.5 fresh crater depth/diameter ratio for Ida (as well as the 1:7 ratio for Gaspra) as real. A single fresh crater at 27°S, 32°E is well-displayed for shadow measurements and a 1:6.5 depth/diameter ratio was obtained. (In Fig. 5 many craters in Palisa Regio appear shadowed and thus amenable to obtaining depths by shadow measurements, but this is an artifact of the image processing.) Unfortunately, checking the photoclinometric results with a statistically significant number of shadow measurements is not possible.

We consider three possible causes for the shallower initial crater depths on Ida (and Gaspra) as compared with larger bodies. First, Carr *et al.* (1994) suggest that on a body as small as Gaspra, whole-body "ringing" and other seismic disturbances from energetic impacts (cf. Nolan *et al.* 1992) could cause (1) more complete collapse of the transient cavity during an impact than on larger bodies, or (2) rapid deterioration of fresh crater rims from shaking by subsequent impacts (i.e., craters might form with 1:5 depth/diameter ratios, but are not found on Gaspra because their rims decay very rapidly immediately after formation). Arguing against the second explanation is the low gravity on small bodies that would provide little cause for collapse of cohesive wall materials, or crater degradation by downslope movement. Crater rims modified by slump scars are not seen on Ida; crater rims appear to remain very circular until other impacts are superposed on them. If pristine craters on Ida are rapidly modified by disturbances triggering collapse of steep walls, these events would have to involve many small, incremental slumps that are too small to be resolved.

A second possibility involves gravitational packing affecting the strength of near-surface materials, and how this change in strength with depth might influence growth of a crater transient cavity. Strength, porosity, and bulk density change dramatically with depth within the upper 0.6 m of lunar regolith (Houston *et al.* 1974, Carrier *et al.* 1992). These changes partly result from gravitational self-loading closing pores and crushing, packing, and interlocking initially more angular particles, along with vibrations from impacts allowing gravity to selectively settle and pack poorly sorted particles. These gravity-related effects should apply over much greater depths through Ida regolith than on the Moon, if a sufficient quantity of loosely cohesive material is present. Gravitational self-loading similar to that affecting the upper 0.6 m of lunar regolith might occur to a depth of about 100 m on a body such as Ida with $g \sim 1$ cm sec^{-2}. Actual changes in material density and strength from purely gravitational crushing probably extend to lesser depths, however, due to expected compaction of near-surface materials from the force of small impacts. In a low gravity setting where a significant increase in material density and strength might occur gradually over relatively great depths, an expanding transient cavity would encounter much weaker and less dense materials in the upper tens of meters (where cavity growth is mostly lateral) than at greater depths (where cavity growth is mostly downward). This would result in growth in depth being impeded by resistance of stronger underlying materials, while lateral growth would proceed further, resulting in a smaller initial depth/diameter ratio.

The third, and most likely, possibility involves ejecta being widely distributed from an impact site on Ida because of low gravity. Smaller craters that are influenced by target strength have ejecta velocities that can be large fractions (or more) of escape velocity under low gravity conditions (Chapman 1976, O'Keefe and Ahrens 1977, Cintala *et al.* 1979, Housen *et al.* 1979a, 1979b, Housen *et al.* 1983, Greenberg *et al.* 1994, Greenberg *et al.* 1996, Asphaug *et al.* 1996). Under these circumstances, less ejecta would pile up on rims, thereby reducing apparent crater depths. This mechanism should be more important on Gaspra, Phobos, and Deimos, all being smaller bodies with less gravity. Craters on Deimos do appear to be shallower than fresh craters on larger rocky bodies, but this is attributable to infilling of debris (Thomas 1979, Thomas and Veverka 1980). It is unclear why wide dispersal of ejecta, or any other process, does not appear to affect the 1:5 depth/diameter ratios of fresh craters on Phobos.

3.3. Dark Floor Craters

Dark floor craters have central interior zones about 10% darker than surrounding terrain, and rims that are 10% brighter (15°N, 25°E, Figs. 2 and 5). Dark floor craters have simple bowl-shaped morphologies similar to other craters on Ida, although brightness variations and resolution limitations reduce the certainty of this observation and make assessment of degradation state uncertain. The interiors of these craters are not concentrically stepped or nested, as would be the case if these impacts had penetrated through a surface layer into (darker) material of greater strength (Oberbeck and Quaide 1967). The dark floors are spectrally similar to surrounding terrain; the same is generally true for the bright rims, except for a few small bluish portions. The most prominent dark floor craters, including Choukoutien, are clustered near 15°N, 25°E. Clustering of these features probably reflects a unique geological setting (as well as favorable illumination conditions) because the bright rims and dark floors of these features maintain their distinctiveness from surrounding terrain and other craters nearby in different spacecraft views over phase angles from 26° to 49°.

Dark floor craters might result from excavation through a brighter surface layer into underlying darker material of similar strength. Lateral compositional heterogeneity on a regional scale would be implied, because nearby craters of similar size do not show dark floors (compare Choukoutien with a crater of similar size at 13°N, 37°E, Figs. 2 and 5). Lunar craters that have penetrated through brighter surface materials into darker, buried mare units display dark halos around their rims (Schultz and Spudis 1979, Hawke and Bell 1981, Bell and Hawke 1984). Dark halo craters of unknown origin also have been identified on Phobos and Deimos (Veverka and Thomas 1979). The idea of explaining dark floor craters on Ida as excavations into underlying darker material derives no additional support from the absence of associated dark ejecta deposits. However, it is unclear whether dark halo deposits on Ida, if they exist, would be visible, given the general difficulties in recognizing all types of continuous ejecta blankets in the images.

Alternatively, dark floor material could represent concentrations of impact melt (cf. Howard and Wilshire 1975, Hawke *et al.* 1979, Smrekar and Pieters 1985, for lunar cases). Goguen *et al.* (1978) proposed that dark deposits within some craters on Phobos are vesicular impact melt, based on the deposits' photometric properties at phase angles ≥80°. However, the mean impact velocity predicted for Ida (3.55 km/sec, Bottke *et al.* 1994) is much lower than for the Moon (13–18 km/sec, Zook 1975), implying less efficient production of impact melt (Ahrens and O'Keefe 1977; Horz and Schaal 1981; Melosh 1989, Fig. 5.3). Along with this difficulty, it is unclear exactly how the local geological setting of the dark floor crater cluster on Ida might lead to enhanced impact melt production or enhanced preservation of melt-rich deposits compared with anywhere else on the asteroid. The explanation might involve how the local setting could preferentially accumulate porous deposits, and how impacts in such deposits should lead to enhanced shock melting compared with impacts in less porous materials (Schaal *et al.* 1979). All dark floor craters identified so far on Ida, and an irregularly shaped dark patch, are found within a very degraded ∼6 km crater at 10°N, 25°E (Figs. 2 and 5). This degraded crater opens onto a protrusion at 20°E that is less cratered than other areas of the surface. Slopes lead down from this protrusion and into the degraded crater containing the dark floor craters. Perhaps a portion of laterally mobile material from the longitude 20°E protrusion has accumulated and concentrated in the interior of the degraded crater, where the crushing of pore space in this deposit in subsequent impacts resulted in enhanced production of glassy impact melt.

4. ISOLATED POSITIVE RELIEF FEATURES

Seventeen isolated positive relief features have been identified on the surface of Ida (see Fig. 9 for examples). The sizes of these features are near the limit of resolution, which varies from 31 to 38 m/pixel in the relevant images. No isolated positive relief features were identified in the 25 m/pixel limb image. The longest dimension of the largest feature is three pixels across (∼150 m). The identification of smaller features, some of which are represented by only a single bright, light-catching pixel, is aided by the presence of associated shadows several pixels in area. Identification of a few features was aided by their location in the limited area of stereo overlap between two high resolution images (Figs. 3 and 4). Isolated positive relief features probably

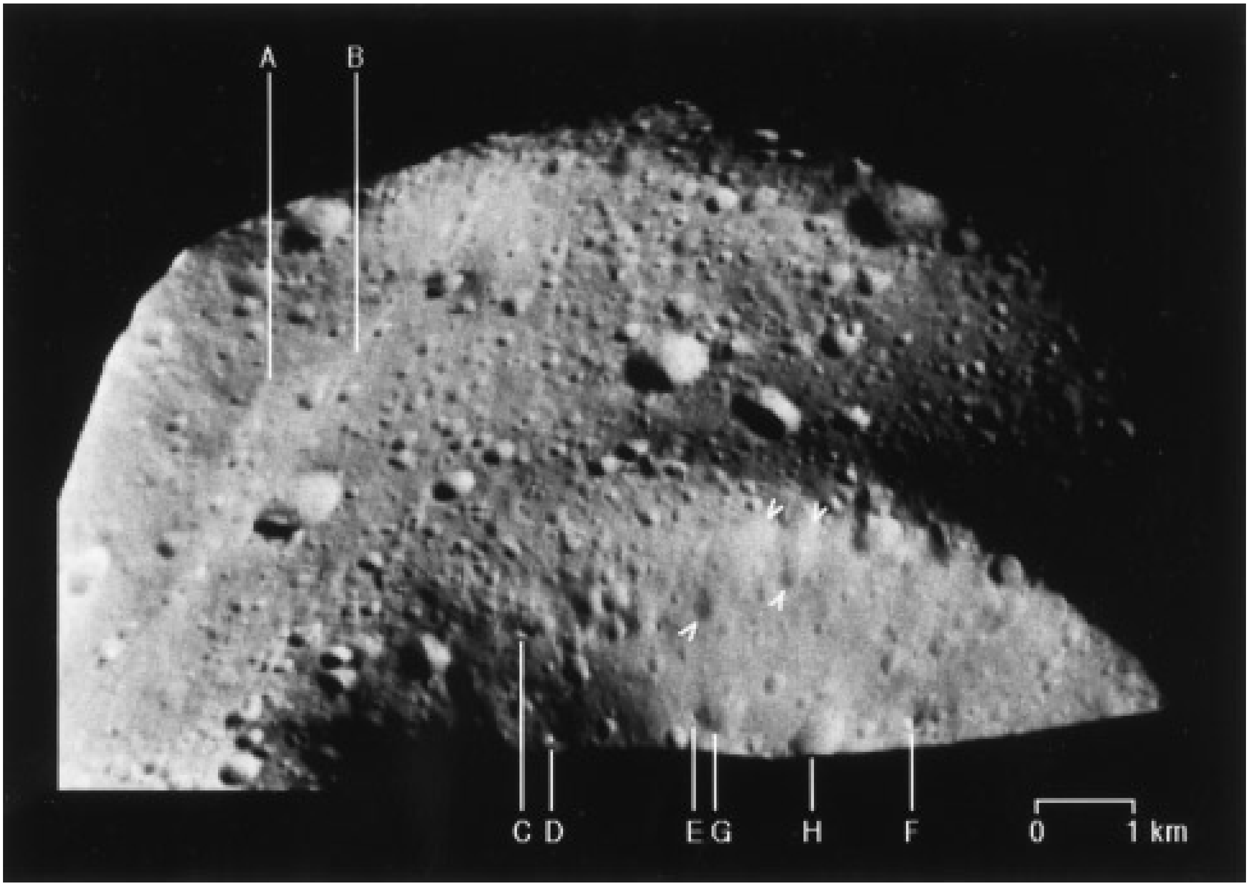

FIG. 9. A portion of image s0202562439 showing the interior of crater Mammoth (see also the upper part of Fig. 3 for different image processing and dynamic height contours). Features discussed in the text include (A) a triangular feature distinguished by higher albedo, bounded on one side by a narrow groove (B); isolated positive relief features that are probably ejecta blocks (C, D, E, and F); asymmetric craters degraded by downslope movement of material (G, H); and chutes with associated craters at their downslope ends (indicated between ><).

represent blocks perched upon or partly embedded in the surface, or perhaps singular outcrops of protruding bedrock.

The distribution of the seventeen isolated positive relief features is not random, and provides clues to possible origins. Twelve of the seventeen features identified are located within two large impact craters (Mammoth and Lascaux) that comprise 4% of the surface. Thirteen of the seventeen features are found on the only leading rotational edge visible at high resolution, and no features are found within 10 km of the rotational axis. However, there is also a resolution dependence that affects the apparent distribution: thirteen of the seventeen features are found on the 31 m/pixel image. When this image is reduced in resolution to 38 m/pixel, about half of the thirteen identified features become ambiguous. We conclude that it is difficult to disentangle possible geological influences on feature distribution, because the better 31 m/pixel image contains both of the block-strewn impact craters and the illuminated rotational leading edge of the asteroid. Nevertheless, two contributing origins are suggested from the feature distribution: (1) as impact products derived directly from the large craters in which most of these features reside (S. Lee *et al.* 1986, P. Lee *et al.* 1996), and (2) as blocks ejected at speeds approaching escape velocity, subsequently swept up preferentially onto the leading rotational edges of the asteroid (Geissler *et al.* 1996).

5. GROOVES

Grooves on Ida are narrow, curvilinear troughs up to 4 km long. Maximum widths are about 350 m, but are commonly 100 m or less. Depths of grooves are estimated to be small fractions of their widths, or less than a few tens of meters. The margins of grooves range from fairly sharp, continuous, parallel crests to beaded outlines. Most grooves are viewed at emission angles greater than 45°, so the appearance of continuous straight margins might be exaggerated. Grooves generally are continuous and do not transform into crater chains or other features anywhere along their lengths, and do not bifurcate or intersect. The grooves are concentrated in and near the crater Lascaux and near craters Mammoth and Kartchner (Figs. 3 and 4), and in this area are subparallel to the long axis of Ida. Grooves on Ida do not occur as clusters of intersecting members as on Phobos (Thomas *et al.* 1979) and Gaspra (Veverka *et al.* 1994), but directional trends are difficult to determine because of restricted lighting geometry at high resolution.

Morphological similarity of grooves on Ida to linear depressions on other small bodies suggests similar origins for all of these features (Thomas and Veverka 1979). Smooth groove cross sections, observed at the limit of resolution, suggest the presence of loose material at least as thick as the grooves are deep. The grooves on Ida are not arranged in any pattern that obviously relates them to one crater or one structural grain, and they trend at a variety of directions to local slopes (calculated by Thomas *et al.* 1996).

Because grooves on Phobos and Gaspra occur in parallel sets that have no consistent relation to local slopes (and those on Phobos even define planes), groove orientations have been hypothesized to reflect internal structure (Thomas *et al.* 1979, Veverka *et al.* 1994). In this hypothesis, the grooves are disturbances in regolith overlying fractures along preferred, nearly planar patterns in deeper, more coherent parts of the object. It is less likely that grooves on Ida represent scars from secondary impacts and rolling boulders, as has been proposed for grooves on Phobos (Head and Cintala 1979, Wilson and Head 1989). For groove morphologies seen on Ida, it seems problematic for large numbers of uniformly sized secondary ejecta clumps to impact the surface at close, evenly spaced intervals at speeds not much more than 10 m/sec, and have sufficient energy to produce trenches of the observed dimensions. Most grooves visible at available resolution are substantially wider than visible blocks and have no blocks at their ends, making formation directly by rolling ejecta blocks unlikely. These ideas are by no means proved, but in any case, the presence of linear depressions on three of the four small objects adequately imaged (Phobos, Deimos, Gaspra, Ida) suggests some general process is responsible for groove formation on small objects.

An important question for the internal fracture hypothesis favored here for grooves on Ida is whether a source crater or craters of suitable size (i.e., energy) and location can be identified. Asphaug *et al.* (1996) performed numerical investigations testing whether stress wave focusing from large impacts could create the grooves observed on Ida, in a manner similar to recent analytical and numerical investigations showing the relation between grooves and the Stickney impact on Phobos (Fujiwara 1991, Asphaug and Melosh 1993, Asphaug and Benz 1994). Grooves on Ida are concentrated at the end antipodal to a 10–15 km diameter saddle-shaped concavity at 10°N, 0°E (Vienna Regio). Asphaug *et al.* carried out three-dimensional numerical calculations using a smooth-particle hydrocode (Benz and Asphaug 1994) applied to an Ida-shaped target that follows the model of Thomas *et al.* (1996). Results predicted surface fracturing in localized areas where the main concentration of grooves is observed on Ida (10°N, 170°E), as well as in a region poorly imaged by Galileo. However, the degraded appearance of the Vienna Regio concavity contrasts with the relatively sharp morphology of the grooves clustered in the 10°N, 170°E area. The 9-km crater Azzurra is less degraded than the Vienna Regio concavity and was also investigated, but only minor surface fracture damage was predicted in the 10°N, 170°E groove area. This led Asphaug *et al.* to propose that fracturing in the area caused by the older Vienna Regio concavity was reactivated later by the Azzurra impact, forming the observed grooves.

6. DEBRIS ON THE SURFACE

Evidence for a layer of debris on Ida derives from analysis of the light scattering properties of the surface, and from high-resolution observations of surface features. The photometric behavior of the surface is consistent with the presence of a blanket of debris (Helfenstein *et al.* 1996). Isolated positive relief features on Ida—probably blocks produced from impacts—represent the largest particle size of ejecta present on the surface (Geissler *et al.* 1996, Lee *et al.* 1996). Bright materials within and around the freshest craters are indicators of particles on the surface produced either by direct deposition of ejecta, or by seismic disturbance of weakly cohesive debris.

Compared with the bright tapered streamers observed on Deimos (Thomas 1979, Thomas and Veverka 1980), evidence on Ida for downslope movement of debris from albedo streaks is much more subtle. Figure 3 shows the interior of the large, relatively degraded crater Lascaux under high sun illumination, along with dynamic slope contours calculated from the shape model of Thomas *et al.* (1996). Subtle light and dark markings seen on the far wall of Lascaux have no recognizable relief and are oriented down local slopes, suggesting movement of debris under the influence of local gravity.

A few craters on the interior wall of crater Mammoth (Figs. 3 and 9) have asymmetric shapes indicative of modification by downslope movement of material. Two other degraded craters in the area (Figs. 3 and 9) have associated shallow, linear depressions oriented upslope, which we term "chutes." Chute lengths range up to 1100 m, and average widths are about one third of lengths. The degraded crater at the downslope end of the largest chute is elongated and has a minimum diameter of 170 m. Centerline depths of chutes are difficult to estimate, but probably range from 20–60 m. We interpret chutes with their associated craters as mass-wasting scars in weakly cohesive material. Each crater cavity provided no support for weak material immediately upslope of its rim, making this material susceptible to downslope movement by seismic accelerations. Failure of this material could have occurred with crater formation, but failure also could have occurred later as a result of seismic shaking of these materials from other impacts. The relatively flat centerline profiles of the chutes are indicative of layer failure (e.g., Bromhead 1986), suggesting an increase in material strength beyond depths of 20–60 m at the time of movement.

A triangular feature that appears brighter than surrounding materials, in spite of complex topographic associations, is located near crater Kartchner and is bounded on its longest side by a groove (5°S, 180°E, Figs. 1, 3, and 9). This feature is seen in several spacecraft views (confirming that it is not just an artifact of slope illumination), but color data are unavailable at useful resolution. Subtle surface texture down the adjacent ridge (on the opposite side of the feature from Kartchner) suggests mass movement has occurred from the ridge down toward the bright feature. The rim of the groove near Kartchner might have acted as a barrier to further movement and dispersal of the deposit. Dynamic slope contours calculated from Thomas *et al.* (1996) show that this feature is located in a local valley—a logical place for a mass-movement deposit to have come to rest.

The favored interpretation of groove morphology on Ida involves the presence of a layer of weakly cohesive debris at the surface (cf. Thomas 1979, Thomas *et al.* 1979 for Phobos, Veverka *et al.* 1994 for Gaspra). (Even if some grooves formed by rolling boulders, an extremely weak debris layer still would be required, such that boulders would leave tracks tens of meters deep under very low Ida gravity.) The depth of this layer can be estimated by assuming that groove depths represent a minimum debris thickness (e.g., Veverka *et al.* 1994). Groove depths on Ida are difficult to estimate directly with available resolution, but are probably a few tens of meters. Assuming groove walls reflect the angle of repose, and using 100 m as a typical width, estimated minimum groove and debris depths are on the order of 30 m.

7. DISCUSSION

Fundamental questions in the geologic analysis of Ida involve the nature of material at the surface, its age (Belton *et al.* 1994, Chapman *et al.* 1996, Greenberg *et al.* 1996), the characteristics of material at depth, and the processes that have produced and continue to affect all of these materials. Some of these issues can be addressed within the limitations of the SSI data, but conclusions are more tentative as we consider materials and processes deeper into the interior. In this section we organize our discussion in terms of constructing a "geologic column" for Ida, which necessarily becomes more speculative with depth. For convenience we divide our discussion between the possible character of regolith, megaregolith, and the deeper interior, but boundaries between these units are almost certainly gradational. The term "regolith" commonly has been used in the discussion of asteroid surfaces to mean any and all impact-derived debris at the surface (e.g., Chapman 1978, Cintala *et al.* 1978, 1979, Housen *et al.* 1979a, 1979b, Housen and Wilkening 1982, Carr *et al.* 1994). For this discussion we use the term in a more restrictive sense: to describe a soil layer that has been overturned many times and "well-gardened" by the impact process. Such layers on the Moon, typically a few meters thick in the maria and <20 m thick in the highlands, evolve over long periods as a result of several related processes and an extremely large number of events. Regolith, in this usage, is distinct from continuous ejecta sheets that are created from a single process in a short time interval (Shoemaker *et al.* 1969, Carrier *et al.* 1992).

The modeling of asteroidal debris layers has a long history, beginning with Chapman (1971). Anders (1975, 1978) evaluated the evidence from solar noble gases implanted in many brecciated meteorites (e.g., Macdougal *et al.* 1974, Poupeau *et al.* 1974) and concluded that many asteroids should have substantial debris layers characterized by blanketing and burial rather than mixing and gardening typical of lunar regolith. Cintala *et al.* (1978, 1979), citing a large body of previous theoretical, experimental, and observational work, concluded that because the slowest moving fractions of crater ejecta are the most likely to be retained on small asteroids, debris layers on these bodies should be depleted in fines compared with lunar soil, resulting in coarser-grained surface debris than found on the Moon. Coarser-grained surface layers on the smaller asteroids was cited by Shaal and Hörz (1977) as an important cause for the general optical immaturity of these surfaces compared with the Moon, because glass production would be less efficient. Matson *et al.* (1977) attributed optical immaturity of asteroid surfaces (relative to the Moon and Mercury) to (1) lower impact velocities resulting in less production of glass, (2) lower gravity causing escape of the highest speed jet of melted ejecta, and (3) in some cases, bulk compositional differences. Cintala *et al.* (1978, 1979) pointed out the importance of seismic shaking from larger impacts on small bodies in periodically churning/lofting surface debris, modifying surface features, and causing downslope migration of loose surface materials. Cintala *et al.* further predicted that these larger impacts would cause significant crushing and fragmentation of subsurface materials similar to the development of lunar megaregolith. Chapman (1978) emphasized for small, rocky bodies how the loss of significant amounts of ejecta to space and "global" distribution of ejecta from large impacts would reduce the number of times a grain of surface debris would be gardened compared with lunar surface materials. Housen *et al.* (1979a) incorporated and developed these points into a detailed model of regolith development for small asteroids, then compared their predictions with a model for regolith development on larger bodies where global dispersal of ejecta did not generally occur (Housen *et al.* 1979b). All of this work leads to the expectation of a layer of debris on the surface of Ida that is coarser, less optically mature, and less gardened throughout its depth than lunar regolith, due to the consequences of much lower gravity and lower impact speeds.

Some of these expectations are confirmed by the SSI images, as already discussed, although these data cannot be used to address the details of asteroid debris layer models. Well-gardened regolith on Ida is probably a very thin surface deposit, compared with the entire thickness of impact-derived debris, and might be restricted from thickening significantly because (1) weakly cohesive material right at the surface is subject to periodic seismic disturbance from large impacts (this process, too, could be considered gardening, but of a much more benign nature than the continuous exposure of more stable surface materials on the Moon to repeated shock, comminution, and alteration by relatively high-speed impacts); and (2) developing regolith is subject to burial by ejecta sheets from distant impacts influenced by target strength. Well-gardened regolith probably grades into volumetrically much more significant deposits of interleaved diffuse ejecta sheets from larger craters (as well as thin surface horizons of more evolved materials that have been buried). These materials presumably grade downward into more stable, even coarser, and more poorly sorted materials that have been brecciated but not ballistically redistributed by impacts. Megaregolith on the Moon is a layer several kilometers thick that is a mixture of ejecta blankets from large impacts and structurally disturbed crust that has been intensely impact-fractured but not overturned or exposed to the surface (Hartmann 1973, Hörz *et al.* 1992). Consistent with much previous work (e.g., Anders 1975, 1978, Cintala 1978, 1979, Housen *et al.* 1979a, 1979b, Housen and Wilkening 1982), we presume the existence of such materials at Ida, grading between well-gardened regolith at the surface and perhaps a more solid interior below. The debris layer of Ida changes into more coherent material somewhere within the megaregolith, perhaps where interleaved ejecta sheets gradually become less common in favor of material that has been brecciated nearly in place, without being overturned.

The transition depths between either the debris layer (or, further down, the megaregolith) and the deeper interior are difficult to determine from morphological clues on the surface. Crater morphology can reveal the transition from surface debris to underlying stronger materials, as long as the strength contrast between layers is significant and the layer interface is narrow (Oberbeck and Quaide 1967). These conditions are met in many areas of the lunar maria where well-gardened regolith overlies basalt bedrock. (In the lunar highlands, the change in strength between regolith and underlying megaregolith is generally not distinct enough to affect crater morphology.) Lunar mare craters <200 m in diameter (seen at high resolution) exhibit variations from simple, bowl-shaped morphology when crater depths penetrate through, or very near to, underlying bedrock. Oberbeck and Quaide (1967) recognized four crater morphologies in the lunar maria and in laboratory simulations: (1) normal bowl-shaped cavities entirely within the overlying weak layer, (2) cavities with a small central-mound floor, (3) flat-floored cavities, and (4) concentrically "benched" cavities that have penetrated entirely through the weak overlying layer and into the stronger substrate. Oberbeck and Quaide (1968) derived relations for calculating regolith thickness from measurements of these morphologies, and determined relative ages of selected areas of the lunar maria (Oberbeck and Quaide 1968, Quaide and Oberbeck 1968). The presence of crater morphologies (2–4) on Ida could indicate strength layering in the near-subsurface. A search for these crater morphologies (limited by much lower resolution than available for the lunar maria) identified no unambiguous examples. There are three possible explanations. First, an abrupt change of material strength might lie too deep to affect the morphology of even the largest undegraded craters. If the largest undegraded craters are around 800 m diameter, the thickness of any weak overlying layer would be $\geq$200 m (Oberbeck and Quaide 1968, Quaide and Oberbeck 1968, Oberbeck *et al.* 1973). Large, fresh craters are scarce, however, making generalizations based on their morphology less reliable. A second possibility is that an abrupt strength transition exists, but the weak, overlying layer is too thin to affect the morphology of the smallest resolved undegraded craters. The smallest craters that can be reliably assessed as undegraded have diameters of about 400 m, and this would constrain the thickness for any overlying weak layer to be $\leq$20 m (Oberbeck and Quaide 1968, Quaide and Oberbeck 1968, Oberbeck *et al.* 1973). The third and most likely possibility is that central mounds, flat bottoms, and concentric benches are absent within craters on Ida because there is no abrupt strength transition like the regolith/bedrock transition in the lunar maria. Increase in strength with depth might be more gradual in a manner analogous to the lunar highlands, where no sharp subsurface interface exists to influence small crater morphology. This scenario is likely because there is no evidence for resurfacing with pristine bedrock that could serve as a substrate for developing a much weaker layer of well-gardened regolith.

Depth/diameter ratios provide a measure of the extent to which craters have been degraded, and allow estimation

TABLE I
Predicted Debris Depths from Five Large Degraded Craters

Crater diameter D (m)	Crater depth d (m)	Initial crater depth (m) assuming d/D of 1:6.5	Initial rim height h_R (m)	Minimum predicted debris depth (m)	Maximum predicted debris depth (m)
1990	180	290	76	34	110
1550	160	240	62	18	80
1320	100	205	53	47	100
1000	80	155	40	35	75
900	65	140	36	39	75

of debris thickness at the surface. Crater obliteration can result from both burial and erosion. Figure 8 suggests that some of the larger craters have decreased in depth by at least 100 m as a result of these two processes. Assuming an initial depth/diameter ratio of 1:6.5, the 1.9-km diameter crater plotted in Fig. 8 has been reduced in depth from ~290 m to ~180 m by some combination of burial and erosion. A conservative estimate of the depth of debris filling this crater is obtained by assuming that erosion is solely responsible for reducing the entire initial rim height. Using $h_R = 0.036D^{1.014}$ (Pike 1977), where h_R is the initial rim height and D is the rim-to-rim diameter, we find that ~76 m in depth reduction, at most, could be attributable solely to erosion, leaving a minimum of ~34 m of depth reduction from the infill of debris. The relationship between D and h_R from Pike (1977) includes the contribution of ejecta (the overturned flap) to the rim height, which may be reduced on Ida due to wider ejecta dispersal under low gravity conditions. An estimate of the maximum possible contribution of burial would assume negligible erosion of the rim and attribute the entire 110 m of depth reduction to infill of debris. Table I summarizes the results of predicted debris thicknesses for five large, degraded craters plotted in Fig. 8. Minimum debris thicknesses are ~20–50 m; maximum thicknesses are ~100 m. These results are similar to estimates for chute depths of 20–60 m and estimates of groove depths of ≥30 m. Together, these estimates suggest that relatively weak, mobile materials lie between the surface and ~50 m depth. This depth probably represents a minimum thickness for the "debris layer," which composes the upper parts of the megaregolith and is dominated by interleaved ejecta sheets and other ballistically emplaced materials. The absence of bluer-than-average craters concentrated on local topographic highs indicates that the mobile component of the debris layer on Ida is thicker and/or more stable than corresponding materials on Gaspra.

Further down, the base of the megaregolith on Ida is expected to be highly variable, as on the Moon. Head (1976) noted that estimates of average megaregolith thickness (Short and Foreman 1972, Hartmann 1973, Hörz *et al.* 1976) coincided with the transition depth between simple craters and more complex crater morphologies. Unfortunately, even if this relationship were indeed causal, it could not be applied to Ida because complex crater morphologies are not seen. Other approaches to determining the depth of the megaregolith must be employed. Numerical investigations of several large impact craters on Ida by Asphaug *et al.* (1996) suggest that intense fracturing of rock beneath large impacts should not occur below depths of about one crater diameter. This suggests typical megaregolith depths of several hundreds of meters to a few kilometers, but extending to depths approaching local Ida radius beneath the largest craters (Mammoth, Lascaux, Undara).

Asphaug and Benz (1994) demonstrated that if Phobos had a mechanically noncoupled interior the shock from the Stickney impact would have attenuated and scattered, preventing the formation of far-field fracture damage (associated with Phobos's grooves). Asphaug *et al.* (1996) note that this effect would be particularly evident for Ida because the distance between their candidate Vienna Regio impact and the nearly antipodal grooves at 10°N, 170°E is much greater than for Phobos; on this basis they concluded that groove formation on Ida by body-transmitted stress waves required the interior to be mechanically coupled. Consistent with this idea is the lack of observational evidence at the surface for reopened seams or joints caused by whole-body flexing or twisting of a nonrigid, multi-component interior structure. The interior of Ida might be largely bedrock or a rigid assemblage of large bedrock fragments that are at least as strong as the lower elements of a megaregolith. The possibility that Ida is megaregolith throughout (e.g., from impact damage into the Koronis parent body) cannot be ruled out. Little more about the deeper interior of Ida can be inferred from features visible at the surface.

8. CONCLUSIONS

(1) The wavelength position of the 1-μm absorption appears stable across the surface, implying that there are no strong variations from region to region in the calcium abundance of pyroxenes or in the pyroxene/olivine ratio.

(2) Relatively blue areas are correlated with areas where the 1-μm absorption is deeper and albedo is higher, as seen as Gaspra and, more distinctly, on the Moon. These areas are mostly associated with bright, undegraded impact craters. A larger blue area at northern latitudes is spectrally indistinguishable from fresh crater materials and probably derives from ballistically emplaced deposits from the crater Azzurra. Blue units and bluer, brighter craters appear randomly across the surface of Ida and are not preferentially located along ridges, as on Gaspra. This suggests that the

debris layer on Ida is not especially thinner along ridges, implying that debris on Ida is less mobile and/or consistently thicker than on Gaspra.

(3) The surface is dominated by impact craters with simple, bowl-shaped morphology. Continuous ejecta blankets cannot be identified, but neither can they be identified surrounding lunar craters at equivalent resolution and lighting/viewing geometry. A complete continuum of crater degradation states is present. Impact craters initially have bluer- and brighter-than-average materials in their interiors and around their rims which darken and redden to average background color and albedo in the first stage of crater degradation. As craters continue to age their rims become more irregular and their depths become shallower as a result of subsequent impacts, until they are hardly recognizable. Color and albedo contrasts of fresh crater deposits originate from the seismic disturbance at impact of the loosely bound optical layer, and from ballistic emplacement of ejecta (albeit more widely dispersed from the smallest craters than on the Moon).

(4) Fresh crater depth/diameter ratios are about 1:6.5, similar to the 1:7 ratios found for fresh craters on Gaspra, but different from the 1:5 ratios found for Phobos and other rocky bodies. Explanations include (a) seismic shaking degrading rims and walls of fresh craters relatively soon after their formation; (b) an extended strength gradient through the near-subsurface, resulting from gradual gravitational packing of loose materials under low gravity which could enhance lateral expansion of the transient cavity relative to its depth; and (c) wider dispersal of ejecta from those crater excavations that are influenced more by target strength than low gravity, resulting in less ejecta piled up at crater rims.

(5) Dark floor craters could be manifestations of a buried compositional heterogeneity (although color properties of the dark floors are the same as materials elsewhere on Ida), or could represent deposits of glassy impact melt similar to dark materials within craters on Phobos.

(6) Isolated positive relief features are probably large blocks of ejecta and are found mostly within two large craters (Lascaux and Mammoth) on the leading rotational edge of the asteroid. This distribution is consistent with two origins: (a) as impact fragments originating directly from the craters where most blocks are found (perhaps as drift weathered from degradation of crater walls), as seen on the Moon; or (b) as blocks ejected from Azzurra at large fractions of escape velocity that have been swept up by rotation of the asteroid.

(7) The morphology of grooves on Ida is most consistent with an origin as internal fractures expressed in a surface layer of less coherent materials.

(8) Morphological evidence for debris at the surface includes resolved ejecta blocks, the contrast in color and albedo of fresh crater materials with surrounding terrain, mass-wasting scars, subtle albedo streaks oriented down some slopes, and grooves.

(9) Because impact is the primary geologic process that has shaped the surface, a simplified lunar-like stratigraphic column of regolith–megaregolith–deeper interior seems applicable, with some modification. The thickness of well-gardened, lunar-like regolith is difficult to determine but is apt to be very thin because of susceptibility to (a) burial by broadly dispersed ejecta sheets, (b) seismic disturbance and mixing with deeper, less evolved materials, and (c) loss to space as high-speed ejecta. The megaregolith of Ida, like on the Moon, is presumed to be dominated by interleaved ejecta sheets near the top, and material that has been intensely fractured and brecciated without being overturned lower down. Within the megaregolith lies the gradational base of the debris layer of materials such as ejecta sheets that have been excavated and emplaced ballistically. Estimates of the average depth of mobile materials derived from chute depths (20–60 m), grooves ($\geq$30 m), and shallowing of the largest degraded craters (20–50 m minimum, ~100 m maximum) suggest a thickness of potentially mobile materials of ~50 m, and a typical thickness for the debris layer of 50–100 m.

ACKNOWLEDGMENTS

We thank Mark Cintala and an anonymous reviewer for very thorough, helpful reviews. We thank Frank Kraljic for helpful discussions, Dan Ball for photographic support, and Larry Bolef and Edisanter Lo for computing assistance. This work was supported by NASA through the Galileo Project at the Jet Propulsion Laboratory.

REFERENCES

Adams, J. B. 1974. Visible and near-infrared diffuse reflectance spectra of pyroxenes as applied to remote sensing of solid objects in the solar system. *J. Geophys. Res.* **79,** 4829–4836.

Adams, J. B., and T. M. McCord 1971. Alteration of lunar optical properties: Age and composition effects. *Science* **171,** 567–571.

Ahrens, T. J., and J. D. O'Keefe 1977. Equations of state and impact-induced shock-wave attenuation on the Moon. In *Impact and Explosion Cratering* (D. J. Roddy, R. O. Pepin, and R. B. Merrill, Eds.), pp. 639–656. Pergamon, New York.

Anders, E. 1975. Do stony meteorites come from comets? *Icarus* **24,** 363–371.

Anders, E. 1978. Most stony meteorites come from the asteroid belt. In *Asteroids: An Exploration Assessment* (D. Morrison and W. C. Wells, ed.), pp. 57–76. NASA Conf. Pub. 2053.

Asphaug, E., and H. J. Melosh 1993. The Stickney impact of Phobos: A dynamical model. *Icarus* **101,** 144–164.

Asphaug, E., and W. Benz 1994. The surface and interior of Phobos. *Lunar Planet. Sci. Conf. XXV,* 43–44.

Asphaug, E., J. M. Moore, D. Morrison, W. Benz, M. C. Nolan, and R. Sullivan 1996. Mechanical and geological effects of impact cratering on Ida. *Icarus* **120,** 158–184.

Bell, J. F., and B. R. Hawke 1984. Lunar dark-haloed impact craters: Origin and implications for early mare volcanism. *J. Geophys. Res.* **89,** 6899–6910.

Belton, M. J. S., J. Veverka, P. Thomas, P. Helfenstein, D. Simonelli, C. Chapman, M. E. Davies, R. Greeley, R. Greenberg, J. Head, S. Murchie, K. Klaasen, T. V. Johnson, A. McEwen, D. Morrison, G. Neukum, F. Fanale, C. Anger, M. Carr, and C. Pilcher 1992. Galileo encounter with 951 Gaspra: First pictures of an asteroid. *Science* **257,** 1647–1652.

Belton, M. J. S., C. R. Chapman, J. Veverka, K. P. Klaasen, A. Harch, R. Greeley, R. Greenberg, J. W. Head III, A. McEwen, D. Morrison, P. C. Thomas, M. E. Davies, M. H. Carr, G. Neukum, F. P. Fanale, D. R. Davis, C. Anger, P. J. Gierasch, A. P. Ingersoll, and C. B. Pilcher 1994. First images of 243 Ida. *Science* **265,** 1543–1547.

Belton, M. J. S., C. R. Chapman, K. P. Klaasen, A. P. Harch, P. C. Thomas, J. Veverka, A. S. McEwen, and R. Pappalardo 1996. Galileo's encounter with 243 Ida: An overview of the imaging experiment. *Icarus* **120,** 1–19.

Benz, W., and E. Asphaug 1994. Impact simulations with fracture. I. Method and tests. *Icarus* **107,** 98–116.

Binzel, R. P. 1988. Collisional evolution in the Eos and Koronis asteroid families: Observational and numerical results. *Icarus* **73,** 303–313.

Binzel, R. P., S. M. Slivan, P. Magnusson, W. Z. Wisniewski, J. Drummond, K. Lumme, M. A. Barucci, E. Dotto, C. Angeli, D. Lazzaro, S. Mottola, M. Gonano-Beurer, T. Michalowski, G. De Angelis, D. J. Tholen, M. DiMartino, M. Hoffmann, E. H. Geyer, F. Velichko 1993a. Asteroid 243 Ida: Groundbased photometry and a pre-Galileo physical model. *Icarus* **105,** 310–325.

Binzel, R. P., S. Xu, and S. J. Bus 1993b. Spectral variations within the Koronis family: Possible implications for the surface colors of asteroid 243 Ida. *Icarus* **106,** 608–611.

Bottke, W. F., M. C. Nolan, R. Greenberg, and R. A. Kolvoord 1994. Velocity distributions among colliding asteroids. *Icarus* **107,** 255–268.

Bromhead, E. N. 1986. *The Stability of Slopes,* pp. 29–132. Surrey Univ. Press, New York.

Carr, M. H., R. L. Kirk, A. McEwen, J. Veverka, P. Thomas, J. W. Head, and S. Murchie 1994. The Geology of Gaspra. *Icarus* **107,** 61–71.

Carrier, W. D. III, G. R. Olhoeft, and W. Mendell 1992. Physical properties of the lunar surface. In *Lunar Sourcebook* (G. Heiken, D. Vaniman, and B. M. French, Eds.), pp. 475–594. Cambridge Univ. Press, New York.

Chapman, C. R. 1971. *Surface Properties of Asteroids.* Ph.D. Thesis. Massachusetts Institute of Technology, Cambridge, MA.

Chapman, C. R. 1976. Asteroids as meteorite parent bodies: The astronomical perspective. *Geochim. Cosmochim. Acta* **40,** 701–719.

Chapman, C. R., D. Morrison, and B. Zellner 1975. Surface properties of asteroids: A synthesis of polarimetry, radiometry, and spectrophotometry. *Icarus* **25,** 104–130.

Chapman, C. R. 1978. Asteroid collisions, craters, regoliths, and lifetimes. In *Asteroids: An Exploration Assessment* (D. Morrison and W. C. Wells, Eds.), pp. 145–160. NASA Conf. Pub. 2053.

Chapman, C. R., P. Paolicchi, V. Zappala, R. P. Binzel, and J. F. Bell 1989. Asteroid families: Physical properties and evolution. In *Asteroids II* (R. P. Binzel, T. Gehrels, and M. S. Mathews, Eds.), pp. 386–415. Univ. of Arizona Press, Tucson.

Chapman, C. R., E. V. Ryan, W. J. Merline, G. Neukum, R. Wagner, P. C. Thomas, J. Veverka, and R. J. Sullivan 1996. Cratering on Ida. *Icarus* **120,** 77–86.

Cintala, M. J., J. W. Head, and J. Veverka 1978. Characteristics of the cratering process on small satellites and asteroids. *Proc. Lunar Planet. Sci. Conf.* **9,** 3803–3830.

Cintala, M. J., and P. J. Mouginis-Mark 1979a. New depth/diameter data for fresh martian craters and some interplanetary comparisons. In *Reports of Planetary Geology Program, 1978–1979,* pp. 182–184. NASA Tech. Mem. 80339.

Cintala, M. J., J. W. Head, and L. Wilson 1979b. The nature and effects of impact cratering on small bodies. In *Asteroids* (T. Gehrels, Ed.), pp. 579–600. Univ. of Arizona Press, Tucson.

Cloutis, E., M. J. Gaffey, T. L. Jackowski, and K. L. Reed 1986. Calibration of phase abundance, composition, and particle size distribution for olivine-orthopyroxene mixtures from reflectance spectra. *J. Geophys. Res.* **91,** 11641–11653.

Cloutis, E. M., and M. J. Gaffey 1991. Pyroxene spectroscopy revisited: Spectral-compositional correlations and relationship to geothermometry. *J. Geophys. Res.* **96,** 22809–22826.

Fujiwara, A. 1991. Stickney-forming impact on Phobos: Crater shape and induced stress distribution. *Icarus* **89,** 384–391.

Gaffey, M. J. 1976. Spectral reflectance characteristics of the meteorite classes. *J. Geophys. Res.* **81,** 905–920.

Gaffey, M. J., J. F. Bell, R. H. Brown, T. H. Burbine, J. L. Piatek, K. L. Reed, and D. A. Chaky 1993. Mineralogical variations within the S-type asteroid class. *Icarus* **106,** 573–602.

Gault, D. E., J. E. Guest, J. B. Murray, D. Dzurisin, and M. C. Malin 1975. Some comparisons of impact craters on Mercury and the Moon. *J. Geophys. Res.* **80,** 2444–2460.

Geissler, P., J.-M. Petit, D. Durda, R. Greenberg, W. Bottke, M. Nolan, and J. Moore 1996. Erosion and ejecta reaccretion on 243 Ida and its Moon. *Icarus* **120,** 140–157.

Goguen, J., J. Veverka, P. Thomas, and T. Duxbury 1978. Phobos: Photometry and origin of dark markings on crater floors. *Geophys. Res. Lett.* **5,** 981–984.

Gradie, J. C., C. R. Chapman, and J. G. Williams 1979. Families of minor planets. In *Asteroids* (T. Gehrels, Ed.), pp. 359–390. Univ. of Arizona Press, Tucson.

Gradie, J. C., C. R. Chapman, and E. F. Tedesco 1989. Distribution of taxonomic classes and the compositional structure of the asteroid belt, In *Asteroids II* (R. P. Binzel, T. Gehrels, and M. S. Mathews, Eds.), pp. 316–335. Univ. of Arizona Press, Tucson.

Greenberg, R., M. C. Nolan, W. F. Bottke, and R. A. Kolvoord 1994. Collisional history of Gaspra. *Icarus* **107,** 84–97.

Greenberg, R., W. Bottke, M. Nolan, P. Geissler, J.-M. Petit, D. Durda, E. Asphaug, and J. Head 1996. Collisional and dynamical history of Ida. *Icarus* **120,** 106–118.

Hartmann, W. J. 1973. Ancient lunar megaregolith and subsurface structure. *Icarus* **18,** 634–639.

Hawke, B. R., D. MacClaskey, and T. B. McCord 1979. Multispectral imaging of lunar crater deposits. In *LPI Contrib. 394,* pp. 50–52. Lunar and Planet. Institute, Houston.

Hawke, B. R., and J. F. Bell 1981. Remote sensing studies of lunar dark-halo impact craters: Preliminary results and implications for early volcanism. *Proc. Lunar Planet. Sci.* **12,** 665–678.

Head, J. W. 1976. The significance of substrate characteristics in determining morphology and morphometry of lunar craters. *Proc. Lunar Sci. Conf.* **7,** 2913–2929.

Head, J. W., and M. J. Cintala 1979. Grooves on Phobos: Evidence for possible secondary cratering origin. In *Reports of the Planetary Geology Program, 1978–1979,* pp. 19–21. NASA Tech. Mem. 80339.

Helfenstein, P., J. Veverka, P. C. Thomas, D. P. Simonelli, P. Lee, K. Klaasen, T. V. Johnson, H. Breneman, J. W. Head, S. Murchie, F. Fanale, M. Robinson, B. Clark, J. Granahan, H. Garbeil, A. S. McEwen, R. L. Kirk, M. Davies, G. Neukum, S. Mottola, R. Wagner, M. Belton, C. Chapman, and C. Pilcher 1994. Galileo photometry of asteroid 951 Gaspra. *Icarus* **107,** 37–60.

Helfenstein, P., J. Veverka, P. C. Thomas, D. P. Simonelli, K. Klaasen, T. V. Johnson, F. Fanale, J. Granahan, A. S. McEwen, M. J. S. Belton, and C. Chapman 1996. Galileo photometry of asteroid 243 Ida. *Icarus* **120,** 48–65.

Hörz, F., R. V. Gibbons, R. E. Hill, and D. E. Gault 1976. Large scale bombardment history of lunar highlands: A Monte Carlo model. *Lunar Science VII,* 381–383.

Hörz, F., and R. B. Schall 1981. Asteroidal agglutinate formation and implications for asteroidal surfaces. *Icarus* **46,** 337–353.

Hörz, F., R. Grieve, G. Heiken, P. Spudis, and A. Binder 1992. Lunar surface processes. In *Lunar Source Book* (G. Heiken, D. Vaniman, and B. M. French, Eds.), pp. 27–120. Cambridge Univ. Press, New York.

Housen, K. R., L. L. Wilkening, C. R. Chapman, and R. Greenberg 1979a. Asteroidal regoliths. *Icarus* **39,** 317–351.

Housen, K. R., L. L. Wilkening, C. R. Chapman, and R. Greenberg 1979b. Regolith development and evolution on asteroids and the Moon. In *Asteroids* (T. Gehrels, Ed.), pp. 601–627. Univ. of Arizona Press, Tucson.

Housen, K. R., and L. L. Wilkening 1982. Regoliths on small bodies in the Solar System. *Ann. Rev. Earth Planet. Sci.* **10,** 355–376.

Housen, K. R., R. M. Schmidt, and K. A. Holsapple 1983. Crater ejecta scaling laws: Fundamental forms based on dimensional analysis. *J. Geophys. Res.* **88,** 2485–2499.

Houston, W. N., J. K. Mitchell, and W. D. Carrier III 1974. Lunar soil density and porosity. *Proc. Lunar Sci. Conf.* **5,** 2361–2364.

Howard, K. A., and H. G. Wilshire 1975. Flows of impact melt at lunar craters. *J. Res. U.S. Geol. Survey* **3,** 237–257.

Kirk, R. L. 1987. *A fast finite-element algorithm for two-dimensional photoclinometry.* Part III of unpublished Ph.D. Dissertation, California Institute of Technology.

Kuiper, G. P. 1950. On the origin of asteroids. *Astron. J.* **55,** 164.

Lee, P., J. Veverka, P. C. Thomas, P. Helfenstein, M. J. S. Belton, C. R. Chapman, R. Greeley, R. Pappalardo, R. Sullivan, and J. W. Head III 1996. Ejecta blocks on 243 Ida and on other asteroids. *Icarus* **120,** 87–105.

Lee, S. W., P. Thomas, and J. Veverka 1986. Phobos, Deimos and the Moon: Size and distribution of ejecta blocks. *Icarus* **68,** 77–86.

McEwen, A. S. 1991. Photometric functions for photoclinometry and other applications. *Icarus* **92,** 298–311.

Macdougal, D., R. S. Rajan, and P. B. Price 1974. Gas-rich meteorites: Possible evidence for origin on a regolith. *Science* **183,** 73–74.

Malin, M. C., and D. Dzurisin 1977. Landform degradation on Mercury, the Moon, and Mars: Evidence from crater depth/diameter relationships. *J. Geophys. Res.* **82,** 376–388.

Matson, D. L., T. V. Johnson, and G. J. Veeder 1977. Soil maturity and planetary regoliths: The Moon, Mercury, and the asteroids. *Proc. Lunar Sci. Conf.* **8,** 1001–1011.

Melosh, H. J. 1989. *Impact Cratering.* Oxford Univ. Press, New York.

Nolan, M. C., E. Asphaug, and R. Greenberg 1992. Numerical simulation of impacts on small asteroids. *Bull. Am. Astron. Soc.* **24,** 959–960.

Oberbeck, V. R., and W. L. Quaide, 1967. Estimated thickness of a fragmental surface layer of Oceanus Procellarum. *J. Geophys. Res.* **72,** 4697–4704.

Oberbeck, V. R., and W. L. Quaide 1968. Genetic implications of lunar regolith thickness variations. *Icarus* **9,** 446–465.

Oberbeck, V. R., W. L. Quaide, M. Mahan, and J. Paulson 1973. Monte Carlo calculations of lunar regolith thickness distributions. *Icarus* **19,** 87–107.

O'Keefe, J. D., and T. J. Ahrens 1977. Meteorite impact ejecta: Dependence of mass and energy lost on planetary escape velocity. *Science* **198,** 1249–1251.

O'Keefe, J. D., and T. J. Ahrens 1993. Planetary cratering mechanics. *J. Geophys. Res.* **98,** 17011–17028.

O'Neil, W. J., N. E. Ausman, T. V. Johnson, and M. R. Landano 1992. *Galileo Completing VEEGA—a Mid-Term Report.* 43rd Congr. Int. Astron. Fed., IAF-92-0560.

Poupeau, G., T. Kirsten, F. Steinbrunn, and D. Storzer 1974. The records of solar wind and solar flares in aubrites. *Earth Planet. Sci. Lett.* **24,** 229–241.

Pieters, C. M., J. B. Adams, P. J. Mouginis-Mark, S. H. Zisk, M. O. Smith, J. W. Head, and T. B. McCord 1985. The nature of crater rays: The Copernicus example. *J. Geophys. Res.* **90,** 12393–12413.

Pike, R. J. 1977. Size-dependence in the shape of fresh impact craters on the Moon. In *Impact and Explosion Cratering* (D. J. Roddy, R. O. Pepin, and R. B. Merrill, Eds.), pp. 489–509. Pergamon, New York.

Pike, R. J. 1980. *Geometric Interpretation of Lunar Craters.* U.S.G.S. Prof. Paper 1046-C, U.S. Government Printing Office, Washington.

Quaide, W. L., and V. R. Oberbeck 1968. Thickness determinations of the lunar surface layer from lunar impact craters. *J. Geophys. Res.* **73,** 5247–5270.

Schaal, R. B., and F. Hörz 1977. Shock metamorphism of lunar and terrestrial basalts. *Proc. Lunar Sci. Conf.* **8,** 1697–1729.

Schaal, R. B., F. Hörz, T. D. Thompson, and J. F. Bauer 1979. Shock metamorphism of granulated lunar basalt. *Proc. Lunar Planet. Sci. Conf.* **10,** 2547–2571.

Schultz, P. H., and P. H. Spudis 1979. Evidence for ancient mare volcanism. *Proc. Lunar Planet Sci. Conf.* **10,** 2899–2918.

Shoemaker, E. M., and R. J. Hackman 1962. Stratigraphic basis for a lunar time scale. In *The Moon* (Kopal, Zdenek, and Mikhailov, Eds.), pp. 289–300. Academic Press, London.

Shoemaker, E. M., E. C. Morris, R. M. Batson, H. E. Holt, K. B. Larson, D. R. Montgomery, J. J. Rennilson, and E. A. Whitaker 1969. Television observations from Surveyor. In *Surveyor Program Results,* pp. 19–128. NASA SP-184.

Short, N. M., and M. L. Foreman 1972. Thickness of impact crater ejecta on the lunar surface. *Mod. Geol.* **3,** 69–91.

Smrekar, S., and C. M. Pieters 1985. Near-infrared spectroscopy of probable impact melt from three large lunar highland craters. *Icarus* **63,** 442–452.

Thomas, P. 1978. *The Morphology of Phobos and Deimos.* Ph.D. Thesis, Cornell University, CRSR Report 693.

Thomas, P. 1979. Surface features of Phobos and Deimos. *Icarus* **40,** 223–243.

Thomas, P., J. Veverka, T. Duxbury, and A. L. Bloom 1979. Grooves on Phobos: Their distribution, morphology, and possible origin. *J. Geophys. Res.* **84,** 8457–8477.

Thomas, P., and J. Veverka 1979. Grooves on asteroids: A prediction. *Icarus* **40,** 394–405.

Thomas, P., and J. Veverka 1980. Downslope movement of material on Deimos. *Icarus* **42,** 234–250.

Thomas, P. C., J. Veverka, D. Simonelli, P. Helfenstein, B. Carcich, M. J. S. Belton, M. E. Davies, and C. Chapman 1994. The shape of Gaspra. *Icarus* **107,** 23–36.

Thomas, P., M. J. S. Belton, B. Carcich, C. R. Chapman, M. E. Davies, R. Sullivan, and J. Veverka 1996. The Shape of Ida. *Icarus* **120,** 20–32.

VEVERKA, J., AND P. THOMAS 1979. Phobos and Deimos: A preview of what asteroids are like? In *Asteroids* (T. Gehrels, Ed.), pp. 628–651. Univ. of Arizona Press, Tucson.

VEVERKA, J., P. THOMAS, T. V. JOHNSON, D. MATSON, AND K. HOUSEN 1986. Physical characteristics of satellite surfaces. In *Satellites* (J. A. Burns and M. S. Mathews, Eds.), pp. 342–402. Univ. of Arizona Press, Tucson.

VEVERKA, J., P. C. THOMAS, D. SIMONELLI, M. J. S. BELTON, M. CARR, C. CHAPMAN, M. E. DAVIES, R. GREELEY, R. GREENBERG, J. HEAD, K. KLAASEN, T. V. JOHNSON, D. MORRISON, AND G. NEUKUM 1994. Discovery of grooves on Gaspra. *Icarus* **107,** 72–83.

VEVERKA, J., P. HELFENSTEIN, P. LEE, P. THOMAS, A. MCEWEN, M. BELTON, K. KLAASEN, T. V. JOHNSON, J. GRANAHAN, F. FANALE, P. GEISSLER, J. W. HEAD III 1996. Ida and Dactyl: Spectral reflectance and color variations. *Icarus* **120,** 66–76.

WEISEL, W. 1978. Fragmentation of asteroids and artificial satellites in orbit. *Icarus* **34,** 99–116.

WILSON, L., AND J. W. HEAD 1989. Dynamics of groove formation on Phobos by ejecta from Stickney. *Lunar. Planet. Sci. Conf. XX,* 1211–1212.

ZELLNER, B., THOLEN, D. J., AND TEDESCO, E. F. 1985. The eight-color asteroid survey: Results for 589 minor planets. *Icarus* **61,** 355–416.

ZOOK, H. A. 1975. The state of meteoritic material on the Moon. *Proc. Lunar Sci. Conf.* **6,** 1653–1672.